

# On the mechanism of soot nucleation. III. The fate and facility of the E-bridge

*Michael Frenklach<sup>\*</sup>, Alexander S. Semnikhin, and Alexander M. Mebel<sup>\*</sup>*

## ABSTRACT

Rotationally-excited dimerization of aromatic moieties is a mechanism proposed recently to explain the initial steps of soot particle inception in combustion and pyrolysis of hydrocarbons. The product of such dimerization, termed E-bridge, is an angled molecular structure composed of two aromatic rings sharing a common bond. The present study explores the immediate fate of the E-bridge. The performed theoretical analysis indicates that abstraction of a bridge H atom by a gaseous H leads to a rapid transformation of the angled to planar structure. The implications of this result is that the collisionally-activated E-bridge formation followed by its flattening effectively increases the size of “planar” aromatic precursors by combining two aromatic moieties with essentially collisional rates, instead of a slower “atom-by-atom” buildup. The faster growth speeds up PAH reaching a size when physical dimerization takes over. The dimerization can be further assisted by the biradicaloid valence structure of the flattened E-bridge.

## 1. INTRODUCTION

Formation of soot in hydrocarbon pyrolysis and combustion remains to be a societal concern due its negative impact on environment and climate. In addition to the societal concern, there is a continuous scientific interest in the phenomenon. The fascination and curiosity with the rapid emergence of carbon particles in flames, exhibited first by Michael Faraday,<sup>1</sup> now crosses multiple disciplines and scientific communities.

Many aspects of the process have been identified and quantified over past few decades. It is now widely accepted that polycyclic aromatic hydrocarbons, PAH, are the precursors to soot particles.<sup>2-3</sup> The subsequent growth of soot particles is also understood at fundamental level: its physical aspects, coagulation, can be described in rigorous mathematical terms and its chemical growth can be represented by elementary chemical reactions.<sup>4-5</sup>

One of the remaining unknowns of the process is particle inception or nucleation, namely, the elementary mechanism of transition from gaseous PAH precursors to solid carbonaceous particles.<sup>4,6</sup> A purely-chemical growth of aromatics, i.e., the extension of PAH size by addition of gaseous species, such as acetylene, is insufficient to explain the size of emerging soot particles; the particle size is determined by particle coagulation.<sup>4</sup> The latter assertion was suggested by early transmission electron microscopy of soot particles<sup>7</sup> and phenomenological analysis of their time evolution,<sup>2</sup> which was later corroborated by detailed modeling.<sup>8-10</sup> A more recent affirmation comes from high-quality experimental observations of particle nanostructure, showing that particle constituents are largely middle-range (four-to-six-ring) PAH.<sup>3, 11-15</sup>

Assuming that the gas-to-solid transition begins with irreversible dimerization of middle-range PAH (like pyrene or coronene) allowed to numerically reproduce the evolution of soot particles in flames.<sup>10, 16-17</sup> However, this assumption appears to be in conflict with the thermodynamic stability of such mid-range PAH dimers.<sup>18-20</sup> Assuming that the dimerization begins with much larger PAH sizes does not reproduce the instant and magnitude of soot appearance in flames. Several alternative proposals for the inception mechanism have been made, most assuming formation of chemically-bonded dimers; all but one of them, in one way or another are not able to reproduce the rate of nucleation, as discussed in a recent publication.<sup>6</sup>

The mechanism that was shown to reproduce the nucleation flux invokes rotational excitation of a dimerization reaction.<sup>6, 21</sup> Development of internal rotation of incoming pyrene molecules during their collision was detected in earlier molecular-dynamics (MD) simulations with on-the-fly quantum (PM3<sup>22</sup>) forces.<sup>23</sup> The internal rotation appeared to serve as a temporary energy accumulator for the excess of the collision translational energy, which slowly dissipates through ro-vibrational energy transfer. The existence of a rotationally/vibrationally-excited complex, one of the keystones of the new model, receives further support from the results of a classical trajectory study of pyrene dimerization performed recently by Chakraborty et al.<sup>24</sup>

While the details of the proposed rotationally-excited dimerization<sup>6</sup> are being scrutinized, the objective of the present study is to investigate the fate of the reaction product, termed E-bridge and illustrated in Figure 1. The E-bridge is composed of two aromatic rings sharing a common bond. The outer aromatic structures, referred hereafter as “wings”, can be activated for subsequent growth (and oxidation) by abstraction of their edge hydrogen atoms.<sup>4, 6</sup> At the same time, a hydrogen atom of one of the bridging carbons can be abstracted as well and the ensued reaction

path is what constitutes the subject of the present theoretical study. The latter entails calculations of the potential energy surface, reaction rate coefficients, and reaction rates at conditions typical of combustion. To facilitate the use of a higher level of quantum theory, we selected the smallest among the E-bridges, the one with the naphthalene wings (the top structure in Figure 1).

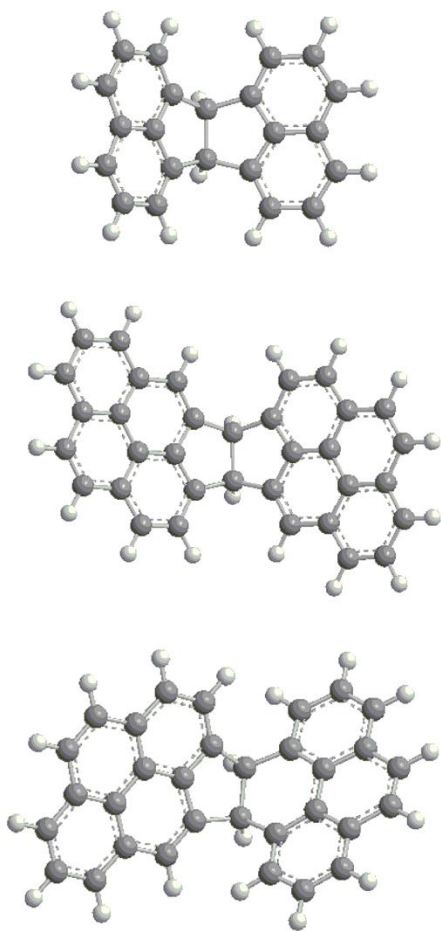


**Figure 1.** Illustration of E-bridge structures.<sup>21</sup>

## 2. CALCULATION METHODS

**2.1. Quantum Chemistry.** We employed here our standard theoretical approach used earlier in the studies of the E-bridge formation. In particular, geometries of the E-bridged molecule with naphthalene wings (structure denoted **r0** in Figure 2) and its radicals formed after H abstractions from various positions in **r0** and consequent isomerization processes (**i1-i7**), as well as transition states and dissociation products were optimized using the density functional theory (DFT) B3LYP method with the 6-311G(d,p) basis set.<sup>25-26</sup> Vibrational frequencies were computed at the same B3LYP/6-311G(d,p) level of theory and were used to evaluate zero-point vibrational energy (ZPE) corrections and for rate constant calculations. The B3LYP calculations were carried out using the GAUSSIAN 09 software package.<sup>27</sup> Single-point energies were further refined using the combined model chemistry G3(MP2,CC) scheme,<sup>28-30</sup> where the energy was evaluated as

$$E[\text{G3(MP2,CC)}] = E[\text{CCSD(T)/6-31G(d)}] + E[\text{MP2/G3Large}] - E[\text{MP2/6-31G(d)}] + \text{ZPE}[\text{B3LYP/6-311G(d,p)}]$$

In this approach, the coupled clusters CCSD(T)/6-31G(d) energy with single and double excitations and perturbative treatment of triple excitations is augmented by the basis set correction  $E[\text{MP2/G3Large}] - E[\text{MP2/6-31G(d)}]$  computed at the 2<sup>nd</sup>-order Møller-Plessett perturbation theory level. The spin-restricted (R) CCSD(T) and MP2 calculations (open-shell, RO, for radicals) were carried out using the MOLPRO 2010 software package.<sup>31</sup>

**2.2. Reaction Rate Coefficients.** Temperature-dependent rate constants for H abstraction by an H atom from C<sub>22</sub>H<sub>14</sub>, **r0**, were computed using conventional transition state theory (TST), whereas temperature- and pressure-dependent rate constants for isomerization and dissociation of the C<sub>22</sub>H<sub>13</sub> radicals were evaluated using the Rice-Ramsperger-Kassel-Marcus Master Equation (RRKM-ME) approach.<sup>32</sup> The MESS software package<sup>33</sup> was utilized for the TST and RRKM-

ME calculations, where partition functions and densities of states for local minima and numbers of states for transition states were computed within the Rigid-Rotor, Harmonic-Oscillator (RRHO) model. The Lennard-Jones parameters  $\epsilon$  and  $\sigma$  for hydrocarbons were adapted from similar-size molecules in the work of Wang and Frenklach,<sup>34</sup> whereas the parameters for the bath gas ( $N_2$ ) were taken from the papers by Vishnyakov et al.<sup>35-36</sup> The collisional energy transfer parameters in RRKM-ME calculations were described within the “exponential down” model,<sup>37</sup> where the temperature dependence of the parameter  $\alpha$  for the deactivating wing of the energy transfer function was expressed as  $\alpha(T) = \alpha_{300} (T/300)^n$ , where  $n = 0.85$  and  $\alpha_{300} = 247 \text{ cm}^{-1}$  are “universal” values proposed by Jasper and Miller for hydrocarbons.<sup>38</sup>

### 3. RESULTS

**3.1. Potential Energy Surface.** The potential energy surface for H abstraction from **r0** by an H atom followed by isomerization and decomposition of the  $C_{22}H_{13}$  radical isomers is shown in Figure 2. It should be noted first that a C-H bond on the E-bridge is significantly weaker than that on a six-membered ring in the naphthalene moiety, namely 86.4 vs. 112.4 kcal/mol. Accordingly, the H abstraction barrier from the bridge is only 6.0 kcal/mol and the formation of  $C_{22}H_{13}$  **i1** +  $H_2$  is 16.8 kcal/mol exothermic. A typical H abstraction barrier from the six-membered ring on the edge of PAH is about 16 kcal/mol<sup>39</sup> and here such a process leads to the formation of **i2** +  $H_2$  residing 9.2 kcal/mol higher in energy than the initial **r0** + H reactants. This means that the E-bridged molecule with naphthalene wings is more likely to decompose by the H loss from the bridge than from a six-membered ring, either unimolecularly or via H abstraction.

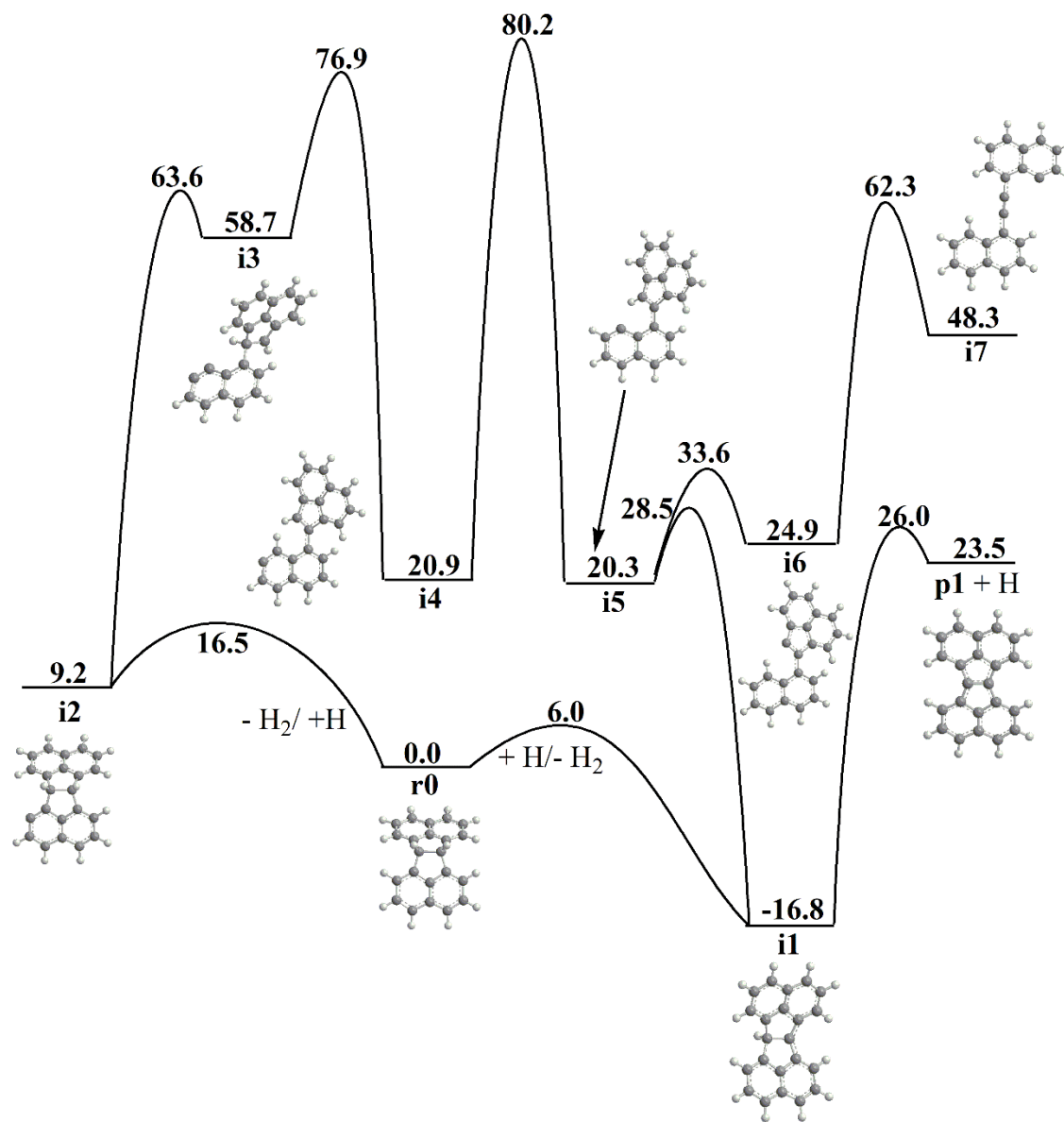


**Figure 2.** Potential energy surface for H abstractions from the E-bridged molecule with naphthalene wings (**r0**) and consequent unimolecular isomerization and decomposition of C<sub>22</sub>H<sub>13</sub> radicals. Relative energies, calculated at the G3(MP2,CC)//B3LYP/6-311G(d,p) + ZPE(B3LYP/6-311G(d,p)) level of theory, are given in kcal/mol.

Next, we consider unimolecular reactions of the C<sub>22</sub>H<sub>13</sub> radicals, **i1** and **i2**, formed as a result of the H abstractions. For **i1**, the most favorable decomposition channel is C-H bond  $\beta$ -scission leading to elimination of the second H atom from the bridge, which is endothermic by 40.3 kcal/mol and proceeds over a barrier of 42.8 kcal/mol. The H loss produces the product **p1**, featuring a planar E-bridge structure with two five-membered rings connecting two naphthalene moieties. The other isomerization channels of **i1** exhibit higher energy demands. C-C bond  $\beta$ -scission breaks one of the five-membered rings forming **i5** via a barrier of 45.3 kcal/mol. Further, **i5** can undergo a facile 1,5-H migration from the five- to six-membered ring with a barrier of only 13.3 kcal/mol to **i6**. The latter can be subjected to a second C-C  $\beta$ -scission rupturing the second five-membered ring and producing **i7**, where the naphthyl radical and naphthalene groups are connected by the acetylene bridge. The intermediate **i7** lies 65.1 kcal/mol above **i1** and the highest barrier on the path to its formation (**i6**  $\rightarrow$  **i7**) is 79.1 kcal/mol relative to **i1** and hence we do not expect this pathway to be competitive with **i1**  $\rightarrow$  **p1** + H. Further decomposition of **i7** is also unlikely because no C-C  $\beta$ -scission is possible, whereas a C-H bond  $\beta$ -scission would result in an aromatic alkyne structure. Therefore, if somehow formed, **i7** would rapidly isomerize back to **i1** or might react with an H atom to close the radical site on the six-membered ring if an encounter occurs during its short lifetime (*vide infra*).

If isomer **i2** is produced, it appears to be much more stable with respect to unimolecular isomerization or decomposition. C-C bond  $\beta$ -scission cleaving a five-membered ring in **i2** producing **i3** requires a barrier as high as 54.4 kcal/mol. Next, a 1,2-H shift in the six-membered ring forming **i4** is relatively easy, with a barrier of 18.2 kcal/mol. However, the second H migration in **i4** connecting it with **i5** and thus providing reaction routes to **i1**, **i7**, and decomposition to **p1** +

H is rather high, 59.3 and 71.0 kcal/mol relative to **i4** and **i2**, respectively. One can therefore anticipate that **i2** would more likely undergo a bimolecular reaction, e.g., back to **r0**, than isomerize to **i1** or dissociate to **p1** + H.

**3.2. Reaction Rate Coefficients.** Figure 3 displays computed rate constants for the reactions controlling the transformation of E-bridge into its planar counterpart. The top panel of Figure 3 presents rate constants calculated for the H abstraction by H from **r0** to produce **i1** in comparison to those evaluated for the formation of **i2** based on a recommended per site H abstraction rate constant from an armchair edge of PAH from our previous work.<sup>39</sup> As anticipated from the much lower barrier for the H abstraction from the E-bridge, the formation of **i1** is preferable over the formation of **i2** up to very high temperatures. For instance, in the 1400–1800 K temperature range, the ratio of the two rate constants is between 9.1 and 4.1, with the rate constant to produce **i1**,  $1.2\text{--}2.8 \times 10^{-11} \text{ cm}^3 \text{ molecule}^{-1} \text{ s}^{-1}$ , growing slower than that to form **i2**,  $1.3\text{--}6.8 \times 10^{-12} \text{ cm}^3 \text{ molecule}^{-1} \text{ s}^{-1}$ .

The middle panel of Figure 3 shows that the unimolecular decomposition of **i1** to **p1** + H is very fast under relevant temperatures with the rate constants being in the range of  $3.5 \times 10^6\text{--}1.1 \times 10^7 \text{ s}^{-1}$  at 1400–1800 K. Thus, once the H abstraction from the E-bridge in **r0** takes place, **i1** would survive only on a microsecond scale at these temperatures. Alternatively, the dominant transformation channel for **i2** in the same temperature interval is predicted to be its isomerization to **i4** with the rate constant of only  $14\text{--}50 \text{ s}^{-1}$ , indicating that the unimolecular reaction of **i2** is too slow to be considered. The rate constant for the reverse direction, **p1** + H → **i1**, is displayed in the bottom panel of Figure 3. It shows a non-monotonic behavior, growing at 1 atm to a maximum of  $3.2 \times 10^{-11} \text{ cm}^3 \text{ molecule}^{-1} \text{ s}^{-1}$  but decreasing in the 1400–1800 K temperature range from  $1.5 \times 10^{-11}$

to  $1.9 \times 10^{-12} \text{ cm}^3 \text{ molecule}^{-1} \text{ s}^{-1}$ . It should be noted that at 1 atm **i7** is predicted to be a chemically stable species only up to 700 K and even at such low temperature, its isomerization rate constant

to **i1** is as high as  $4.3 \times 10^7 \text{ s}^{-1}$ .

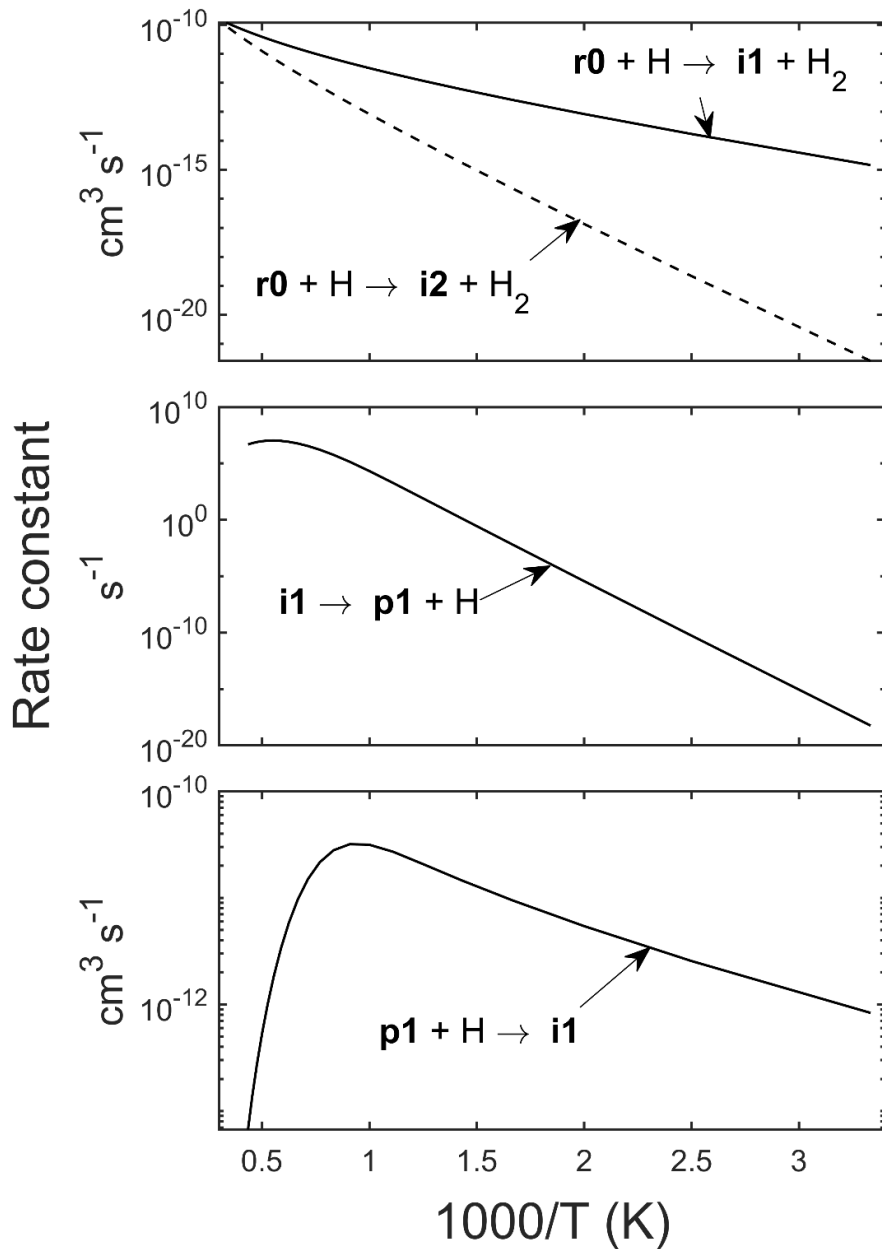


**Figure 3.** Calculated rate constants; top panel:  $\mathbf{r0} + \mathbf{H} \rightarrow \mathbf{i1/i2} + \mathbf{H_2}$  reactions, middle panel: unimolecular decomposition  $\mathbf{i1} \rightarrow \mathbf{p1} + \mathbf{H}$  at 1 atm, bottom panel: its reverse,  $\mathbf{p1} + \mathbf{H} \rightarrow \mathbf{i1}$  reaction at 1 atm.

**3.3. Kinetic Analysis.** To test the kinetic implications of the E-bridge flattening pathway examined here, we solved a set of ordinary differential equations for the three-step reaction model detailed in Table 1. The differential equations were solved with the rate coefficients computed at a constant temperature and with constant values of gaseous species concentrations of H and H<sub>2</sub>. Figure 4 displays the results obtained for two sets of initial conditions typical of soot particle appearance in laminar premixed flames.<sup>6</sup>

**Table 1. Rate Coefficients of the Three-Step Reaction Model<sup>a</sup>**

| Temperature<br>(K) | (R1) $\mathbf{r0} + \mathbf{H} \rightleftharpoons \mathbf{i1} + \mathbf{H_2}$ |   | (R2) $\mathbf{r0} \rightleftharpoons \mathbf{i1} + \mathbf{H}$ |   | (R3) $\mathbf{i1} \rightleftharpoons \mathbf{p1} + \mathbf{H}$ |   |
|--------------------|---|---|--|---|--|---|
|                    | forward<br>(cm <sup>3</sup> s <sup>-1</sup> )                                 | reverse<br>(cm <sup>3</sup> s <sup>-1</sup> ) | forward<br>(s <sup>-1</sup> )                                  | reverse<br>(cm <sup>3</sup> s <sup>-1</sup> ) | forward<br>(s <sup>-1</sup> )                                  | reverse<br>(cm <sup>3</sup> s <sup>-1</sup> ) |
| 1200               | 6.7×10 <sup>-12</sup>   | 3.6×10 <sup>-16</sup>                         | 1.6×10 <sup>-3</sup>   | 3.5×10 <sup>-13</sup>                         | 5.7×10 <sup>5</sup>  | 2.8×10 <sup>-11</sup>                         |
| 1500               | 1.5×10 <sup>-11</sup>   | 3.3×10 <sup>-15</sup>                         | 1.5×10 <sup>-1</sup>   | 2.0×10 <sup>-14</sup>                         | 5.9×10 <sup>6</sup>  | 9.7×10 <sup>-12</sup>                         |
| 1800               | 2.8×10 <sup>-11</sup>   | 1.6×10 <sup>-14</sup>                         | 1.3  | 1.4×10 <sup>-15</sup>                         | 1.1×10 <sup>7</sup>  | 1.9×10 <sup>-12</sup>                         |
| 2200               | 5.1×10 <sup>-11</sup>   | 7.3×10 <sup>-14</sup>                         | 4.2  | 5.3×10 <sup>-17</sup>                         | 6.3×10 <sup>6</sup>  | 1.4×10 <sup>-13</sup>                         |

<sup>a</sup>The rate-constant values for the entire temperature range, 300–2800 K, is given in the Supporting Information.

Inspection of the results depicted in Figure 4 indicates that E-bridge is almost entirely converted at 1500 K into the planar structure by about 0.1 ms. This time decreases to ~0.01 ms as temperature increased to 1800 K and to ~1 μs with an additional increase in the H mole fraction

to 0.01. The latter set of conditions is typical of the gaseous environment in the main flame zone and the one at 1500 K represents those of soot nucleation.<sup>6</sup> Considering that at these conditions the growth of the naphthalene ring occurs on the time scale of  $\sim 1$  ms,<sup>40</sup> the E-bridge should flatten before any consequential interaction takes place.

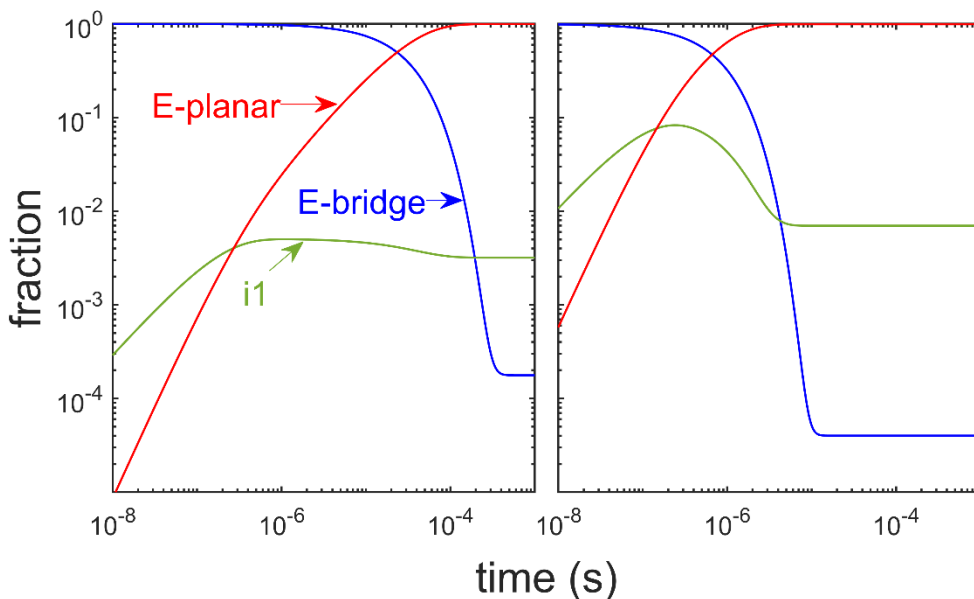


**Figure 4.** Conversion fractions of the reactant, E-bridge (**r0**), intermediate radical (**i1**), and product, E-planar (**p1**), computed at pressure 1 atm and mole fraction of H<sub>2</sub> 0.1; left panel: temperature 1500 K and H mole fraction 0.0004, right panel: temperature 1800 K and H mole fraction 0.01.

Another feature to note in Figure 4 is that E-bridge does not decay completely with time but its concentration reaches a plateau. The asymptotic E-planar-to-E-bridge ratio can be estimated through reduced equilibrium constants,<sup>6</sup> namely,

$$\frac{[\text{E-planar}]}{[\text{E-bridge}]} = K_{1-2}K_3 = \frac{k_1[\text{H}]}{k_{-1}[\text{H}_2] + k_{-2}[\text{H}]} \frac{k_3}{k_{-3}[\text{H}]}$$

where  $k_i$  is the rate constant of reaction  $R(i)$ , with positive subscript for the forward and negative for the reverse directions, and  $K_i$  is the reduced equilibrium constant for step  $i$ . For instance, at the first set of conditions in Figure 1 ( $T = 1500$  K,  $x_{\text{H}} = 0.0004$ ,  $x_{\text{H}_2} = 0.1$ ) this ratio is  $5.6 \times 10^3$  and for the second set ( $T = 1800$  K,  $x_{\text{H}} = 0.01$ ,  $x_{\text{H}_2} = 0.1$ ) it is  $2.4 \times 10^4$ .

#### 4. CONCLUSIONS AND IMPLICATIONS

The present analysis indicates that the angled structure of E-bridge should quickly flatten in flame environments. E-bridge was suggested to form in a rotationally-excited reaction of two PAHs, a radical and an edge five-membered ring—the process suggested to explain the initial stages of soot particle inception in hydrocarbon flames.<sup>6</sup> The flattening transformation following the formation of E-bridge is so rapid that adding this step to the previously examined two-step model should not affect the principle kinetic outcome, the development of a meaningful nucleation flux, as indeed was verified by a computational test.

The mechanism of rotational excitation has been the only one able of explaining the nucleation time scale. Another critical prerequisite for a successful mechanism is being able to explain the transition from the two-dimensional geometry of PAH precursors to the three-dimensional geometry of nascent soot particles. The formation of angled structures, like those shown in Figure 1, was thought<sup>6</sup> to initiate such a transition. The found now flattening of E-bridge brings the initial presumption to further scrutiny.

While the flattening of E-bridge may seem like putting an end to the build-up of a three-dimensional structure in an otherwise rate-efficient nucleation pathway, the net outcome of the collisionally-activated E-bridge formation followed by E-bridge flattening is to effectively increase the size of “planar” aromatic precursors by combining two aromatic moieties with essentially collisional rates, instead of a slower “atom-by-atom” buildup. This faster growth speeds up PAH reaching a size when physical dimerization takes over.<sup>3, 20, 41-43</sup>

There is another interesting feature of the flattened E-bridge that could add to its efficacy. The structure of the planar E-bridge can be viewed as a substituted ethylene: a double C=C bond bridging two multi-ring moieties, the wings. There are two vibrations of the wings, symmetric ( $59\text{ cm}^{-1}$ ) and antisymmetric ( $68\text{ cm}^{-1}$ ), flipping them around the bridging C=C bond and thereby bending the ethylenic construct. It is known that bending ethylene results in a biradicaloid valence structure.<sup>44</sup> Moreover, the vertical singlet-triplet gap in the planar E-bridge, computed here at the B3LYP/6-311G(d,p) level, is only 35.1 kcal/mol, almost 70 kcal/mol lower than the corresponding value for ethylene, 104.7 kcal/mol. On this basis, we expect the flattened E-bridge to exhibit an increased radical activity, which, among other things, may offer stronger attractive forces in clustering into three-dimensional soot structural units. This feature and associated phenomenon shall be subjects of a future investigation.

**Supporting Information:** (a) Table S1 containing calculated rate constants for relevant reactions resulting in E-bridge flattening at 1 atm and (b) input file for RRKM-ME calculations on the  $\text{C}_{22}\text{H}_{13}$  PES following H abstractions for the E-bridge using the MESS package, which includes optimized Cartesian coordinates, vibrational frequencies and relative energies of all structures.

## AUTHOR INFORMATION

### Corresponding Authors

**Michael Frenklach** — *Department of Mechanical Engineering, University of California, Berkeley, California 94720-1740, USA; orcid.org/0000-0002-9174-3306; Email: [frenklach@berkeley.edu](mailto:frenklach@berkeley.edu)*

**Alexander M. Mebel** — *Department of Chemistry and Biochemistry, Florida International University, Miami, Florida 33199, USA; orcid.org/0000-0002-7233-3133; Email: [mebela@fiu.edu](mailto:mebela@fiu.edu)*

### Author

**Alexander S. Semenikhin** — *Samara National Research University, Samara, 443086, Russia.*

### Funding Sources

US Department of Energy, Basic Energy Sciences, the grant DE-FG02-04ER15570 to FIU; Ministry of Education and Science of the Russian Federation, the grant No. 14.Y26.31.0020 to Samara University.

## ACKNOWLEDGMENTS

The work at Florida International University was funded by the US Department of Energy, Basic Energy Sciences under the grant DE-FG02-04ER15570. A.M.M. also acknowledges the Instructional & Research Computing Center (IRCC, web: <http://ircc.fiu.edu>) at FIU for providing HPC computing resources that have contributed to the research results reported within this paper. The work at Samara University was supported by the by the Ministry of Education and Science of the Russian Federation under the grant No. 14.Y26.31.0020.

## REFERENCES

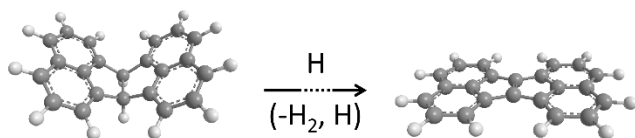
- (1) Faraday, M., *The Chemical History of a Candle*. Oxford University: New York, 2011.
- (2) Haynes, B. S.; Wagner, H. G., Soot formation. *Prog. Energy Combust. Sci.* **1981**, *7*, 229-273.
- (3) Jacobson, R. S.; Korte, A. R.; Vertes, A.; Miller, J. H., The Molecular Composition of Soot. *Angew. Chem. Int. Ed.* **2020**, *59*, 4484-4490.
- (4) Frenklach, M., Reaction mechanism of soot formation in flames. *Phys. Chem. Chem. Phys.* **2002**, *4*, 2028–2037.
- (5) Whitesides, R.; Frenklach, M., Detailed kinetic Monte Carlo simulations of graphene-edge growth. *J. Phys. Chem. A* **2010**, *114*, 689–703.
- (6) Frenklach, M.; Mebel, A. M., On the mechanism of soot nucleation. *Phys. Chem. Chem. Phys.* **2020**, *22*, 5314-5331.
- (7) Donnet, J.-B., Fifty years of research and progress on carbon black. *Carbon* **1994**, *32*, 1305-1310.
- (8) Frenklach, M.; Ebert, L. B., Comment on the proposed role of spheroidal carbon clusters in soot formation. *J. Phys. Chem.* **1988**, *92*, 561-563.
- (9) Frenklach, M.; Clary, D. W.; Gardiner, W. C., Jr.; Stein, S. E., Detailed kinetic modeling of soot formation in shock-tube pyrolysis of acetylene. *Proc. Combust. Inst.* **1985**, *20*, 887-901.
- (10) Appel, J.; Bockhorn, H.; Frenklach, M., Kinetic modeling of soot formation with detailed chemistry and physics: Laminar premixed flames of C<sub>2</sub> hydrocarbons. *Combust. Flame* **2000**, *121*, 122–136.
- (11) Schulz, F.; Commodo, M.; Kaiser, K.; De Falco, G.; Minutolo, P.; Meyer, G.; D'Anna, A.; Gross, L., Insights into incipient soot formation by atomic force microscopy. *Proc. Combust. Inst.* **2019**, *37*, 885-892.
- (12) Commodo, M.; Kaiser, K.; De Falco, G.; Minutolo, P.; Schulz, F.; D'Anna, A.; Gross, L., On the early stages of soot formation: Molecular structure elucidation by high-resolution atomic force microscopy. *Combust. Flame* **2019**, *205*, 154-164.
- (13) Carbone, F.; Canagaratna, M. R.; Lambe, A. T.; Jayne, J. T.; Worsnop, D. R.; Gomez, A., Exploratory analysis of a sooting premixed flame via on-line high resolution (API-TOF) mass spectrometry. *Proc. Combust. Inst.* **2019**, *37*, 919-926.
- (14) Faccinetto, A.; Irimiea, C.; Minutolo, P.; Commodo, M.; D'Anna, A.; Nuns, N.; Carpentier, Y.; Pirim, C.; Desgroux, P.; Focsa, C.; Mercier, X., Evidence on the formation of dimers of polycyclic aromatic hydrocarbons in a laminar diffusion flame. *Communications Chemistry* **2020**, *3*, 112.
- (15) Do, H.-Q.; Tran, L.-S.; Gasnot, L.; Mercier, X.; El Bakali, A., Experimental study of the influence of hydrogen as a fuel additive on the formation of soot precursors and particles in atmospheric laminar premixed flames of methane. *Fuel* **2021**, *287*, 119517.

- (16) Frenklach, M.; Wang, H., Detailed modeling of soot particle nucleation and growth. *Proc. Combust. Inst.* **1991**, *23*, 1559-1566.
- (17) Hou, D.; Lindberg, C. S.; Manuputty, M. Y.; You, X.; Kraft, M., Modelling soot formation in a benchmark ethylene stagnation flame with a new detailed population balance model. *Combust. Flame* **2019**, *203*, 56-71.
- (18) Sabbah, H.; Biennier, L.; Klippenstein, S. J.; Sims, I. R.; Rowe, B. R., Exploring the role of PAHs in the formation of soot: Pyrene dimerization. *J. Phys. Chem. Lett.* **2010**, *1*, 2962-2967.
- (19) Elvati, P.; Violi, A., Thermodynamics of poly-aromatic hydrocarbon clustering and the effects of substituted aliphatic chains. *Proc. Combust. Inst.* **2013**, *34*, 1837-1843.
- (20) Menon, A.; Martin, J. W.; Akroyd, J.; Kraft, M., Reactivity of Polycyclic Aromatic Hydrocarbon Soot Precursors: Kinetics and Equilibria. *J. Phys. Chem. A* **2020**, *124*, 10040-10052.
- (21) Semenikhin, A. S.; Savchenkova, A. S.; Chechet, I. V.; Matveev, S. G.; Frenklach, M.; Mebel, A. M., On the mechanism of soot nucleation. II. E-bridge formation at the PAH bay. *Phys. Chem. Chem. Phys.* **2020**, *22*, 17196-17204.
- (22) Stewart, J. J. P., Optimization of parameters for semiempirical methods I. Method. *J. Comput. Chem.* **1989**, *10*, 209-220.
- (23) Schuetz, C. A.; Frenklach, M., Nucleation of soot: Molecular dynamics simulations of pyrene dimerization. *Proc. Combust. Inst.* **2003**, *29*, 2307-2314.
- (24) Chakraborty, D.; Lischka, H.; Hase, W. L., Dynamics of Pyrene-Dimer Association and Ensuing Pyrene-Dimer Dissociation. *J. Phys. Chem. A* **2020**, *124*, 8907-8917.
- (25) Lee, C. T.; Yang, W. T.; Parr, R. G., Development of the Colle-Salvetti correlation-energy formula into a functional of the electron density. *Phys. Rev. B* **1988**, *37*, 785-789.
- (26) Becke, A. D., Density-functional thermochemistry. III. The role of exact exchange. *J. Chem. Phys.* **1993**, *98*, 5648-5652.
- (27) Frisch, M. J.; Trucks, G. W.; Schlegel, H. B.; Scuseria, G. E.; Robb, M. A.; Cheeseman, J. R.; Scalmani, G.; Barone, V.; Mennucci, B.; Petersson, G. A.; Nakatsuji, H.; Caricato, M.; Li, X.; Hratchian, H. P.; Izmaylov, A. F.; Bloino, J.; Zheng, G.; Sonnenberg, J. L.; M. Hada; Ehara, M.; Toyota, K.; Fukuda, R.; Hasegawa, J.; Ishida, M.; Nakajima, T.; Honda, Y.; Kitao, O.; Nakai, H.; Vreven, T.; J. A. Montgomery, J.; Peralta, J. E.; Ogliaro, F.; Bearpark, M.; Heyd, J. J.; E. Brothers; Kudin, K. N.; Staroverov, V. N.; Keith, T.; Kobayashi, R.; J. Normand; Raghavachari, K.; Rendell, A.; Burant, J. C.; Iyengar, S. S.; Tomasi, J.; Cossi, M.; Rega, N.; Millam, J. M.; Klene, M.; Knox, J. E.; Cross, J. B.; Bakken, V.; Adamo, C.; Jaramillo, J.; Gomperts, R.; Stratmann, R. E.; Yazyev, O.; Austin, A. J.; Cammi, R.; Pomelli, C.; Ochterski, J. W.; Martin, R. L.; Morokuma, K.; Zakrzewski, V. G.; G. A. Voth; Salvador, P.; Dannenberg, J. J.; Dapprich, S.; Daniels, A. D.; Farkas, O.; Foresman, J. B.; Ortiz, J. V.; Cioslowski, J.; Fox, D. J. *Gaussian 09*, revision B.01; Gaussian, Inc.: Wallingford CT, 2010.
- (28) Baboul, A. G.; Curtiss, L. A.; Redfern, P. C.; Raghavachari, K., Gaussian-3 theory using density functional geometries and zero point energies. *J. Chem. Phys.* **1999**, *110*, 7650-7657.

- (29) Curtiss, L. A.; Raghavachari, K.; Redfern, P. C.; Baboul, A. G.; Pople, J. A., Gaussian-3 theory using coupled cluster energies. *Chem. Phys. Lett.* **1999**, *314*, 101–107.
- (30) Curtiss, L. A.; Redfern, P. C.; Raghavachari, K.; Rassolov, V.; Pople, J. A., Gaussian-3 theory using reduced Møller-Plesset order. *J. Chem. Phys.* **1999**, *110*, 4703-4709.
- (31) Werner, H.-J.; Knowles, P. J.; Kinizhia, G.; Manby, F. R.; Schutz, M.; Celani, P.; Korona, T.; Lindh, R. *MOLPRO, version 2010.1.*, 2010.1; Ab Initio Programs: Lexington, MA, 2010.
- (32) Georgievskii, Y.; Miller, J. A.; Burke, M. P.; Klippenstein, S. J., Reformulation and solution of the master equation for multiple-well chemical reactions. *J. Phys. Chem. A* **2013**, *117*, 12146-12154.
- (33) Georgievskii, Y.; Klippenstein, S. J. *Master Equation System Solver (MESS)*, available online at <https://github.com/PACChem/MESS>, 2016.3.23; 2015.
- (34) Wang, H.; Frenklach, M., Transport properties of polycyclic aromatic hydrocarbons for flame modeling. *Combust. Flame* **1994**, *96*, 163–170.
- (35) Vishnyakov, A.; Debenedetti, P. G.; Neimark, A. V., Statistical geometry of cavities in a metastable confined fluid. *Phys. Rev. E* **2000**, *62*, 538-544.
- (36) Ravikovitch, P. I.; Vishnyakov, A.; Neimark, A. V., Density functional theories and molecular simulations of adsorption and phase transition in nanopores. *Phys. Rev. E* **2001**, *64*, 011602.
- (37) Troe, J., Theory of thermal unimolecular reactions at low pressures. I. Solutions of the master equation. *J. Chem. Phys.* **1977**, *66*, 4745-4757.
- (38) Jasper, A. W.; Miller, J. A., Theoretical unimolecular kinetics for  $\text{CH}_4 + \text{M} \rightleftharpoons \text{CH}_3 + \text{H} + \text{M}$  in eight baths,  $\text{M} = \text{He}, \text{Ne}, \text{Ar}, \text{Kr}, \text{H}_2, \text{N}_2, \text{CO},$  and  $\text{CH}_4$ . *J. Phys. Chem. A* **2011**, *115*, 6438-6455.
- (39) Semenikhin, A. S.; Savchenkova, A. S.; Chechet, I. V.; Matveev, S. G.; Liu, Z.; Frenklach, M.; Mebel, A. M., Rate constants for H abstraction from benzo(a)pyrene and chrysene: a theoretical study. *Phys. Chem. Chem. Phys.* **2017**, *19*, 25401-25413.
- (40) Savchenkova, A. S.; Chechet, I. V.; Matveev, S. G.; Frenklach, M.; Mebel, A. M., Formation of phenanthrenyl radicals via the reaction of acenaphthyl with acetylene. *Proc. Combust. Inst.* **2021**, *38*, 1441-1448.
- (41) Herdman, J. D.; Miller, J. H., Intermolecular potential calculations for polynuclear aromatic hydrocarbon clusters. *J. Phys. Chem. A* **2008**, *112*, 6249-6256.
- (42) Botero, M. L.; Adkins, E. M.; González-Calera, S.; Miller, H.; Kraft, M., PAH structure analysis of soot in a non-premixed flame using high-resolution transmission electron microscopy and optical band gap analysis. *Combust. Flame* **2016**, *164*, 250-258.
- (43) Botero, M. L.; Sheng, Y.; Akroyd, J.; Martin, J.; Dreyer, J. A. H.; Yang, W.; Kraft, M., Internal structure of soot particles in a diffusion flame. *Carbon* **2019**, *141*, 635-642.
- (44) Weiner, B.; Skokov, S.; Frenklach, M., A theoretical analysis of a diamond (100)-(2x1) dimer bond. *J. Chem. Phys.* **1995**, *102*, 5486-5491



# COVER ART



# Supporting Information

## On the Mechanism of Soot Nucleation. III. The Fate and Facility of the E-Bridge

*Michael Frenklach*<sup>\*1</sup>, *Alexander S. Semenukhin*<sup>2</sup>, and *Alexander M. Mebel*<sup>\*3</sup>

<sup>1</sup> *Department of Mechanical Engineering, University of California, Berkeley, California 94720-1740, USA; orcid.org/0000-0002-9174-3306; Email: [frenklach@berkeley.edu](mailto:frenklach@berkeley.edu)*

<sup>2</sup> *Samara National Research University, Samara, 443086, Russia*

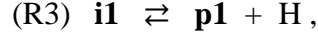
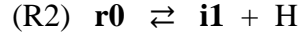
<sup>3</sup> *Department of Chemistry and Biochemistry, Florida International University, Miami, Florida 33199, USA; orcid.org/0000-0002-7233-3133; Email: [mebela@fiu.edu](mailto:mebela@fiu.edu)*

The material contains:

- a) Reaction model used in the simulations of the reaction system studied.
- b) Reaction rate constants computed in the present studies, Table **S1**
- c) Input data for the reaction-rate calculations

## Kinetic Model

The kinetic model used in our analysis is a three-step reaction system,



with the corresponding set of differential equations (ODE) given as

$$\begin{cases} \frac{df_{r0}}{dt} = -k_1[\text{H}]f_{r0} + k_{-1}[\text{H}_2]f_{i1} - k_2f_{r0} + k_{-2}[\text{H}]f_{i1} \\ \frac{df_{i1}}{dt} = k_1[\text{H}]f_{r0} - k_{-1}[\text{H}_2]f_{i1} + k_2f_{r0} - k_{-2}[\text{H}]f_{i1} - k_3f_{i1} + k_{-3}[\text{H}]f_{p1} \\ \frac{df_{p1}}{dt} = k_3f_{i1} - k_{-3}[\text{H}]f_{p1} \end{cases}$$

where  $k_i$  is the reaction rate constant, whose positive subscript,  $i$ , designates the forward and negative,  $-i$ , the reverse directions of reaction (Ri).  $f_{r0}$ ,  $f_{i1}$ , and  $f_{p1}$  are the concentration ratios of  $\mathbf{r0}$ ,  $\mathbf{i1}$ , and  $\mathbf{p1}$  at time  $t$  relative to the initial concentration of  $\mathbf{r0}$  at  $t = 0$ , i.e.,

$$f_{r0} = \frac{[\mathbf{r0}]_t}{[\mathbf{r0}]_{t=0}}; \quad f_{i1} = \frac{[\mathbf{i1}]_t}{[\mathbf{r0}]_{t=0}}; \quad \text{and} \quad f_{p1} = \frac{[\mathbf{p1}]_t}{[\mathbf{r0}]_{t=0}}$$

$[\text{H}]$  and  $[\text{H}_2]$  are the concentrations of gaseous H and  $\text{H}_2$ , respectively, and their products with the corresponding  $k$ 's form the pseudo-first-order rate constants, in the units of  $\text{s}^{-1}$ .

The ODE system was solved with the initial conditions of  $f_{r0} = 1$ ,  $f_{i1} = 0$ , and  $f_{p1} = 0$ , constant  $[\text{H}]$  and  $[\text{H}_2]$  with values listed in the caption of Figure 4 of the manuscript, and the rate constant values listed in Table S1.

**Table S1.** Calculated Rate Constants for Relevant Reactions Resulting in E-bridge Flattening at 1 Atm.<sup>a</sup>

| T (K) | E-bridge + H<br>→ <b>i1</b> + H <sub>2</sub> | <b>i1</b> + H <sub>2</sub> → E-<br>bridge + H | E-bridge → <b>i1</b> + H <sup>b</sup> | <b>i1</b> + H → E-bridge <sup>b</sup> | <b>i1</b> → <b>p1</b> + H | <b>p1</b> + H → <b>i1</b> |
|-------|--|---|---------------------------------------|---------------------------------------|---------------------------|---------------------------|
| 300   | 1.46E-15                                     | 1.29E-28                                      | 5.74E-49                              | 1.06E-10                              | 5.68E-19                  | 8.33E-13                  |
| 400   | 1.72E-14                                     | 1.34E-24                                      | 4.64E-33                              | 1.02E-10                              | 5.35E-11                  | 2.55E-12                  |
| 500   | 8.40E-14                                     | 3.69E-22                                      | 1.43E-23                              | 8.28E-11                              | 3.63E-06                  | 5.43E-12                  |
| 600   | 2.58E-13                                     | 1.64E-20                                      | 2.34E-17                              | 5.42E-11                              | 6.40E-03                  | 9.47E-12                  |
| 700   | 6.01E-13                                     | 2.59E-19                                      | 4.79E-13                              | 2.94E-11                              | 1.38E+00                  | 1.46E-11                  |
| 800   | 1.17E-12                                     | 2.12E-18                                      | 6.15E-10                              | 1.38E-11                              | 7.93E+01                  | 2.07E-11                  |
| 900   | 2.03E-12                                     | 1.12E-17                                      | 1.24E-07                              | 5.91E-12                              | 1.83E+03                  | 2.70E-11                  |
| 1000  | 3.22E-12                                     | 4.38E-17                                      | 6.86E-06                              | 2.38E-12                              | 2.11E+04                  | 3.15E-11                  |
| 1100  | 4.78E-12                                     | 1.37E-16                                      | 1.50E-04                              | 9.25E-13                              | 1.39E+05                  | 3.19E-11                  |
| 1200  | 6.74E-12                                     | 3.60E-16                                      | 1.64E-03                              | 3.55E-13                              | 5.74E+05                  | 2.80E-11                  |
| 1300  | 9.13E-12                                     | 8.30E-16                                      | 1.07E-02                              | 1.36E-13                              | 1.64E+06                  | 2.16E-11                  |
| 1400  | 1.20E-11                                     | 1.73E-15                                      | 4.66E-02                              | 5.23E-14                              | 3.50E+06                  | 1.50E-11                  |
| 1500  | 1.52E-11                                     | 3.30E-15                                      | 1.49E-01                              | 2.04E-14                              | 5.90E+06                  | 9.67E-12                  |
| 1600  | 1.90E-11                                     | 5.88E-15                                      | 3.71E-01                              | 8.14E-15                              | 8.27E+06                  | 5.83E-12                  |
| 1700  | 2.32E-11                                     | 9.90E-15                                      | 7.60E-01                              | 3.31E-15                              | 9.99E+06                  | 3.36E-12                  |

|      |          |          |          |          |          |          |
|------|----------|----------|----------|----------|----------|----------|
| 1800 | 2.79E-11 | 1.59E-14 | 1.33E+00 | 1.38E-15 | 1.07E+07 | 1.86E-12 |
| 1900 | 3.31E-11 | 2.44E-14 | 2.04E+00 | 5.89E-16 | 1.04E+07 | 1.01E-12 |
| 2000 | 3.87E-11 | 3.62E-14 | 2.82E+00 | 2.58E-16 | 9.38E+06 | 5.30E-13 |
| 2100 | 4.49E-11 | 5.21E-14 | 3.57E+00 | 1.16E-16 | 7.91E+06 | 2.73E-13 |
| 2200 | 5.15E-11 | 7.30E-14 | 4.20E+00 | 5.32E-17 | 6.32E+06 | 1.38E-13 |
| 2300 | 5.85E-11 | 9.98E-14 | 4.67E+00 | 2.51E-17 | 4.82E+06 | 6.69E-14 |
| 2400 | 6.60E-11 | 1.34E-13 | 4.94E+00 | 1.21E-17 |          |          |
| 2500 | 7.40E-11 | 1.76E-13 | 5.01E+00 | 6.00E-18 |          |          |
| 2600 | 8.24E-11 | 2.27E-13 | 4.91E+00 | 3.03E-18 |          |          |
| 2700 | 9.13E-11 | 2.89E-13 | 4.67E+00 | 1.57E-18 |          |          |
| 2800 | 1.01E-10 | 3.62E-13 | 4.34E+00 | 8.27E-19 |          |          |
| 2900 | 1.10E-10 | 4.49E-13 | 3.96E+00 | 4.46E-19 |          |          |
| 3000 | 1.20E-10 | 5.51E-13 | 3.54E+00 | 2.45E-19 |          |          |

<sup>a</sup>In units of  $\text{cm}^3 \text{s}^{-1}$  and  $\text{s}^{-1}$  for bimolecular and unimolecular reactions, respectively.

<sup>b</sup>Evaluated using phase space theory with the calculated C-H bond dissociation of 86.4 kcal/mol.

**Input file for RRKM-ME calculations on the C<sub>22</sub>H<sub>13</sub> PES following H abstractions from the E-bridge using the MESS package**

```

TemperatureList[K]          300 400 500 600 700 800 900 1000
1100 1200 1300 1400 1500 1600 1700 1800 1900 2000 2100 2200 2300 2400
2500 2600 2700 2800 2900 3000
PressureList[atm]           0.01 0.03 0.1 0.3 1. 3. 10. 30.
100.
EnergyStepOverTemperature   0.2          #Ratio of discretization
energy step to T
ExcessEnergyOverTemperature 30
ModelEnergyLimit[kcal/mol]  400
WellCutoff                  10
ChemicalEigenvalueMax      0.2
ChemicalEigenvalueMin      1.e-6          #only for direct
diagonalization method
CalculationMethod           direct
EigenvalueOutput            eigenvalue.out
Reactant                    #ground energy of bimolecular species will be used as a
reference.
Model
  EnergyRelaxation
    Exponential
      Factor[1/cm]          247
      Power                 0.85
      ExponentCutoff        15
    End
  CollisionFrequency
    LennardJones
      Epsilons[1/cm]        101.5  834.9  ! N2 pyrene-Frenklach
      Sigmas[angstrom]      3.6154 7.24  ! N2 pyrene-Frenklach
      Masses[amu]           28.  277.31312
    End
  OutputTemperatureStep[K]  100
  OutputTemperatureSize    20
  OutputReferenceEnergy[kcal/mol] 0.
  Well          W1 # i2
  Species
RRHO
Geometry[angstrom]  35
C      1.295906      1.152238      0.552077
C      3.773302      -1.318357     -0.784996
C      3.107073      2.380538     -0.454199
C      3.766431      1.223493     -0.81342
C      1.283167      -1.203221     0.58821
C      0.006259      0.786945     1.275997

```

|   |           |           |           |
|---|-----------|-----------|-----------|
| C | 1.864646  | 2.362624  | 0.235298  |
| C | 3.210425  | -0.045239 | -0.496448 |
| C | 1.972571  | -0.029166 | 0.185639  |
| C | -0.005263 | -0.809891 | 1.2941    |
| C | -1.286522 | -1.189993 | 0.567388  |
| C | -1.960786 | -0.013655 | 0.182389  |
| C | 3.115892  | -2.475962 | -0.398515 |
| C | 1.893363  | -2.371418 | 0.276775  |
| C | -1.841096 | -2.408888 | 0.261788  |
| C | -3.080678 | -2.439995 | -0.432439 |
| C | -3.745198 | -1.290026 | -0.807093 |
| C | -3.194968 | -0.016117 | -0.504555 |
| C | -1.283729 | 1.164484  | 0.55956   |
| C | -3.749385 | 1.255749  | -0.808914 |
| C | -1.847083 | 2.380450  | 0.256628  |
| C | -3.08896  | 2.407608  | -0.434476 |
| H | 4.722682  | -1.384311 | -1.306658 |
| H | 4.715303  | 1.278019  | -1.336324 |
| H | 0.012793  | 1.192399  | 2.292871  |
| H | -0.011948 | -1.197747 | 2.317167  |
| H | 3.547610  | -3.446623 | -0.617435 |
| H | -1.352946 | -3.338695 | 0.531912  |
| H | -3.516206 | -3.403875 | -0.672781 |
| H | -4.691741 | -1.355489 | -1.333206 |
| H | -4.696667 | 1.317786  | -1.334091 |
| H | -1.369624 | 3.314929  | 0.529976  |
| H | -3.528824 | 3.370157  | -0.672281 |
| H | 1.388484  | 3.300797  | 0.498274  |
| H | 3.548884  | 3.339456  | 0.702185  |

Core RigidRotor

SymmetryFactor 0.5

End

Frequencies[1/cm] 99

|       |         |         |         |         |         |         |         |         |       |
|-------|---------|---------|---------|---------|---------|---------|---------|---------|-------|
| 28.93 | 58.93   | 102.13  | 155.76  | 165.27  | 193.66  | 239.38  | 253.29  | 278.12  |       |
|       | 315.94  | 428.8   | 430.64  | 438.26  | 459.92  | 472.69  | 476.9   | 513.06  |       |
|       | 519.99  | 527.29  | 555.29  | 579.31  | 581.81  | 585.49  | 627.19  | 635.74  | 682.5 |
|       | 693.2   | 697.97  | 735.35  | 762.79  | 763.97  | 780.84  | 797.69  | 804.49  |       |
|       | 815.26  | 825.63  | 852.34  | 862.7   | 881.1   | 900.05  | 915.14  | 918.68  |       |
|       | 930.63  | 953.16  | 968.75  | 977.5   | 980.9   | 985.91  | 1037.67 | 1043.08 |       |
|       | 1049.22 | 1066.58 | 1077.53 | 1109.82 | 1133.43 | 1170.07 | 1179.03 | 1184.86 |       |
|       | 1197.65 | 1202.46 | 1231.18 | 1237.73 | 1243.15 | 1248.78 | 1259.92 | 1270.79 |       |
|       | 1276.89 | 1286.81 | 1330.11 | 1370.24 | 1382.47 | 1390.04 | 1421.6  | 1440.87 |       |
|       | 1448.06 | 1462.76 | 1485.39 | 1500.37 | 1507.74 | 1530.81 | 1596.56 | 1626.24 |       |
|       | 1635.43 | 1640.35 | 1646.25 | 1660.24 | 3033.34 | 3048.12 | 3158.16 | 3158.53 |       |
|       | 3159.27 | 3160.23 | 3169.87 | 3171.64 | 3172.07 | 3175.02 | 3182.52 | 3183.61 |       |
|       | 3184.17 |         |         |         |         |         |         |         |       |

```

ZeroEnergy[kcal/mol] 0
ElectronicLevels[1/cm] 1
    0 2
    End
    End
    Well      W2 # i3
Species
RRHO
Geometry[angstrom] 35
C      -2.41132      -0.052952      -0.308938
C      -3.585734     -0.302947      0.513545
C      -4.88753      0.125214      0.091996
C      -5.122831     0.794243     -1.099838
C      -3.92442      0.980463     -1.802195
C      -2.785389     0.627566     -1.484725
C      -1.127142     -0.476409     0.102627
C      -1.007045     -1.138344     1.310966
C      -2.128793     -1.389239     2.123311
C      -3.387973     -0.984621     1.738607
C      3.552002      0.705139      0.252901
C      2.358083      0.124138     -0.202801
C      2.262661     -1.197337     -0.762641
C      3.450023     -1.95115      -0.858595
C      4.650592     -1.378418     -0.405844
C      4.726528     -0.097901     0.136101
C      3.444666      2.018855     0.775288
C      2.214037      2.654187     0.81401
C      1.028890      2.039632     0.342485
C      1.112487      0.760624     -0.170781
C      0.082116     -0.194195     -0.777396
C      0.924960     -1.419692     -1.099907
H      -5.726947     -0.088601     0.746358
H      -6.109369     1.113642     -1.40793
H      -0.027359     -1.468906     1.638068
H      -1.994484     -1.909995     3.064655
H      -4.243356     -1.186586     2.373956
H      3.447082     -2.953022     -1.272167
H      5.561732     -1.962548     -0.481962
H      5.682036      0.291305     0.470239
H      4.328824      2.526965     1.145589
H      2.152923      3.658842     1.218104
H      0.086487      2.573532     0.392217
H      -0.300385     0.239281     -1.714012
H      0.509597      -2.315047     1.542169
    Core      RigidRotor
SymmetryFactor 0.5

```

End  
 Frequencies[1/cm] 99  
 10.55 39.58 58.77 144.49 152.49 170.66 172.58 208.46 223.8  
 267.63 302.15 394.92 415.31 423.28 447.32 456.89 464.81  
 480.19 510.55 513.89 528.27 543.47 550.38 566.25 595.83  
 620.58 639.98 668.61 681.13 693.04 728.18 749.47 753.82  
 769.81 781.05 801.96 808.39 828.18 836.21 847.57 864.6  
 873.66 915.08 926.44 945.61 952.27 971.63 981.72 986.98  
 1019.07 1031.35 1052.61 1068.92 1085.67 1111.6 1127.14 1139.32  
 1174.25 1174.84 1192.28 1204.03 1206.03 1220.74 1226.91 1241.89  
 1259.6 1275.79 1318.25 1332.64 1337.33 1365.75 1377.07 1401.47  
 1421.36 1425.27 1457.95 1466.65 1474.32 1513.59 1521.51 1573.6  
 1576.65 1621.46 1635.84 1638.1 2048.51 2970.33 3159.05 3159.86  
 3161.43 3165.15 3172.83 3174.17 3175.08 3184.4 3185.31 3187.2  
 3203.05 3211.86

ZeroEnergy[kcal/mol] 49.5  
 ElectronicLevels[1/cm] 1  
 0 2

End  
 End  
 Well W3 # i4

Species  
 RRHO  
 Geometry[angstrom] 35  
 C 2.378424 -0.289222 0.053867  
 C 3.704692 0.241927 -0.092747  
 C 4.822423 -0.501525 0.375761  
 C 4.663582 -1.726143 0.98948  
 C 3.354790 -2.180391 1.133021  
 C 2.231758 -1.547832 0.718797  
 C 1.262001 0.473116 -0.432974  
 C 1.499274 1.719901 -0.990273  
 C 2.801487 2.240523 -1.123987  
 C 3.882960 1.513769 -0.694258  
 C -3.716876 0.294207 0.33389  
 C -2.418515 -0.059194 -0.033884  
 C -2.050624 -1.295728 -0.613642  
 C -3.046425 -2.220806 -0.850318  
 C -4.384951 -1.889348 -0.498218  
 C -4.725219 -0.679351 0.076546  
 C -3.868203 1.580538 0.926237  
 C -2.762302 2.387745 1.113441  
 C -1.450461 1.990424 0.729355  
 C -1.278966 0.756796 0.137633  
 C -0.124142 -0.027089 -0.372494  
 C -0.59937 -1.236278 -0.808924

|   |           |           |           |
|---|-----------|-----------|-----------|
| H | 5.815820  | -0.083196 | 0.245166  |
| H | 5.515397  | -2.294268 | 1.34516   |
| H | 1.243054  | -1.95452  | 0.889108  |
| H | 0.660253  | 2.293177  | -1.367051 |
| H | 2.941842  | 3.213271  | -1.581491 |
| H | 4.889411  | 1.903323  | -0.804044 |
| H | -2.835529 | -3.189563 | -1.290747 |
| H | -5.163637 | -2.620308 | -0.686055 |
| H | -5.758586 | -0.472142 | 0.333606  |
| H | -4.849777 | 1.924719  | 1.234601  |
| H | -2.891897 | 3.361100  | 1.573502  |
| H | -0.615919 | 2.658021  | 0.912124  |
| H | -0.002452 | -2.015845 | -1.261726 |

Core RigidRotor

SymmetryFactor 0.5

End

Frequencies[1/cm] 99

|       |         |         |         |         |         |         |         |         |       |  |
|-------|---------|---------|---------|---------|---------|---------|---------|---------|-------|--|
| 29.26 | 49.93   | 60.44   | 145.66  | 163.56  | 168.55  | 178.47  | 219.87  | 233.83  |       |  |
|       | 279.42  | 317.99  | 393.9   | 407.83  | 436.39  | 456.31  | 464.08  | 482.65  |       |  |
|       | 507.14  | 519.35  | 537.24  | 539.89  | 564.85  | 585.64  | 605.76  | 634.25  |       |  |
|       | 646.83  | 653.47  | 691.66  | 700.12  | 737.03  | 754.6   | 766.92  | 768.37  |       |  |
|       | 785.05  | 790.94  | 818.92  | 823.21  | 827.44  | 837.74  | 871.75  | 882.16  | 920.5 |  |
|       | 923.83  | 928.87  | 935.93  | 959.18  | 976.6   | 984.01  | 986.87  | 999.45  |       |  |
|       | 1037.27 | 1053.13 | 1058.76 | 1072.31 | 1094.84 | 1130.37 | 1150.13 | 1172.26 |       |  |
|       | 1193.67 | 1202.47 | 1207.9  | 1222.82 | 1240.27 | 1248.38 | 1264.47 | 1284.8  |       |  |
|       | 1300.9  | 1334.63 | 1353.36 | 1382.35 | 1385.22 | 1405.9  | 1446.71 | 1449.7  |       |  |
|       | 1457.46 | 1473.68 | 1488.22 | 1514.29 | 1516.12 | 1560.07 | 1596.52 | 1615.97 |       |  |
|       | 1631.29 | 1639.76 | 1650.79 | 1658.41 | 3153.93 | 3160.49 | 3161.73 | 3162.12 |       |  |
|       | 3170.48 | 3174.08 | 3176.04 | 3179.22 | 3183.88 | 3186.14 | 3186.23 | 3188.52 |       |  |
|       | 3215.54 |         |         |         |         |         |         |         |       |  |

ZeroEnergy[kcal/mol] 11.7

ElectronicLevels[1/cm] 1

0 2

End

End

Well W4 # i5

Species

RRHO

Geometry[angstrom] 35

|   |          |           |           |
|---|----------|-----------|-----------|
| C | 2.363895 | -0.221254 | 0.014487  |
| C | 3.698494 | 0.314401  | -0.058982 |
| C | 4.796003 | -0.506146 | 0.318593  |
| C | 4.614516 | -1.794993 | 0.758001  |
| C | 3.303990 | -2.342086 | 0.845929  |
| C | 2.275718 | -1.53699  | 0.482586  |
| C | 1.241095 | 0.592799  | -0.353344 |

|   |           |           |           |
|---|-----------|-----------|-----------|
| C | 1.480820  | 1.895237  | -0.762518 |
| C | 2.786723  | 2.421698  | -0.832588 |
| C | 3.872585  | 1.653411  | -0.491301 |
| C | -3.752956 | 0.224564  | 0.256408  |
| C | -2.424855 | -0.077326 | -0.046598 |
| C | -1.970036 | -1.334865 | -0.508121 |
| C | -2.903107 | -2.334318 | -0.693267 |
| C | -4.269053 | -2.055441 | -0.409531 |
| C | -4.695451 | -0.824571 | 0.052088  |
| C | -3.998464 | 1.539429  | 0.744092  |
| C | -2.946277 | 2.419476  | 0.90708   |
| C | -1.601585 | 2.072245  | 0.595334  |
| C | -1.337322 | 0.814227  | 0.094317  |
| C | -0.124667 | 0.056100  | -0.31649  |
| C | -0.520591 | -1.210929 | -0.663395 |
| H | 5.795510  | -0.089247 | 0.256667  |
| H | 5.466318  | -2.403402 | 1.042796  |
| H | 3.151720  | -3.357606 | 1.195045  |
| H | 0.647335  | 2.514354  | -1.070138 |
| H | 2.927965  | 3.443082  | -1.167882 |
| H | 4.876753  | 2.060814  | -0.544257 |
| H | -2.621316 | -3.322468 | -1.041183 |
| H | -4.998615 | -2.844115 | -0.557029 |
| H | -5.746573 | -0.658229 | 0.262808  |
| H | -5.008103 | 1.846777  | 0.99551   |
| H | -3.144808 | 3.413642  | 1.29201   |
| H | -0.815672 | 2.798160  | 0.768267  |
| H | 0.132622  | -1.989761 | -1.029287 |

Core RigidRotor

SymmetryFactor 0.5

End

Frequencies[1/cm] 99

|       |         |         |         |         |         |         |         |         |       |
|-------|---------|---------|---------|---------|---------|---------|---------|---------|-------|
| 35.55 | 51.2    | 67.42   | 141.59  | 164.02  | 168.56  | 178.28  | 218.35  | 235.44  |       |
|       | 275.93  | 311.31  | 393.14  | 424.45  | 439.95  | 456.69  | 463.78  | 477.44  | 509.2 |
|       | 518.83  | 535.17  | 552.33  | 565.1   | 593.06  | 605.92  | 630.16  | 647.16  |       |
|       | 650.84  | 688.73  | 697.01  | 739.42  | 751.72  | 765.23  | 771.76  | 784.65  |       |
|       | 798.71  | 816.73  | 820.53  | 827.66  | 837.66  | 864.35  | 885.09  | 919.25  |       |
|       | 923.53  | 928.24  | 935.15  | 972.28  | 976.39  | 985.91  | 988.36  | 996.14  |       |
|       | 1038.97 | 1042.42 | 1060.87 | 1081.63 | 1092.56 | 1129.97 | 1164.09 | 1173.01 |       |
|       | 1188.16 | 1198.56 | 1204.93 | 1215.94 | 1236.9  | 1245.22 | 1258.13 | 1284.84 |       |
|       | 1308.13 | 1348.96 | 1357.25 | 1383.37 | 1396.36 | 1407.08 | 1449.06 | 1453.59 |       |
|       | 1457.31 | 1472.77 | 1487.4  | 1507.98 | 1516.61 | 1556.14 | 1586.2  | 1628.75 |       |
|       | 1630.61 | 1649    | 1652.72 | 1658.36 | 3156.81 | 3160.36 | 3160.77 | 3161.87 |       |
|       | 3167.75 | 3170.84 | 3175.51 | 3178.06 | 3180.76 | 3183.79 | 3187.54 | 3195.5  |       |
|       | 3223.15 |         |         |         |         |         |         |         |       |

ZeroEnergy[kcal/mol] 11.1

```

ElectronicLevels[1/cm]      1
      0      2
      End
      End
      Well      W5 # i1
Species
RRHO
Geometry[angstrom]      35
C      1.193557      0.325080      1.366157
C      -1.29798      -0.437842      4.044109
C      2.413051      -0.285626      3.347637
C      1.249440      -0.470722      4.068943
C      -1.177516      0.349645      1.323612
C      0.781642      0.849152      0.0
C      2.404622      0.123183      1.988712
C      -0.013701      -0.260843      3.454844
C      0.006562      0.140585      2.106799
C      -0.742493      0.654622      0.0
C      -1.177516      0.349645      -1.323612
C      0.006562      0.140585      -2.106799
C      -2.446195      -0.23733      3.293271
C      -2.414071      0.144843      1.93538
C      -2.414071      0.144843      -1.93538
C      -2.446195      -0.23733      -3.293271
C      -1.29798      -0.437842      -4.044109
C      -0.013701      -0.260843      -3.454844
C      1.193557      0.325080      -1.366157
C      1.249440      -0.470722      -4.068943
C      2.404622      0.123183      -1.988712
C      2.413051      -0.285626      -3.347637
H      -1.375741      -0.740677      5.082697
H      1.297194      -0.785177      5.106142
H      0.990016      1.932870      0.0
H      -3.411428      -0.385413      3.765631
H      -3.341767      0.281267      1.392634
H      -3.341767      0.281267      -1.392634
H      -3.411428      -0.385413      -3.765631
H      -1.375741      -0.740677      -5.082697
H      1.297194      -0.785177      -5.106142
H      3.344679      0.263786      -1.466936
H      3.367992      -0.45737      -3.832325
H      3.344679      0.263786      1.466936
H      3.367992      -0.45737      3.832325
      Core      RigidRotor
SymmetryFactor 1
      End

```

```

Frequencies[1/cm]      99
51.79  52.95  115.13 162.88 172.37 195.35 228.35 245.26 270.91
      325.09 374.06 423.88 434.7  469.16 478.88 479.44 487.6  516.1
      523.75 554.39 573.53 590.52 591.42 637.25 648.53 651.61
      686.93 724.8  737.13 753.58 761.77 781.96 785.93 800.22
      806.74 810.54 828.01 854.41 874.99 885.04 904.51 916.25
      918.77 953.41 972.7  974.22 981.02 982.01 1028.34 1039.75
      1042.85 1068.01 1076.13 1092.55 1104.59 1156.67 1164.8 1176.4
      1184.5  1194.92 1202.33 1230.51 1238.26 1243.27 1249.75 1282.46
      1290.51 1349.87 1366.03 1380.56 1386.34 1401.93 1420.22 1424.99
      1455.36 1460.57 1465.41 1475.01 1516.26 1517.95 1585.77 1606.99
      1620.91 1623.61 1639.83 1647.84 2945.83 3158.97 3159.36 3160.34
      3160.66 3170.45 3171.88 3175.79 3176.65 3182.94 3183.91 3187.5
      3189.81

```

```
ZeroEnergy[kcal/mol] -26.0
```

```
ElectronicLevels[1/cm]      1
```

```
0 2
```

```
End
```

```
End
```

```
Well      W6 # i6
```

```
Species
```

```
RRHO
```

```

Geometry[angstrom]      35
C  0.8343659766  -2.182972479  -0.8122316194
C  0.5325416302  -3.4916742099  -1.3143186239
C  1.5416062006  -4.4898261792  -1.3020059574
C  2.7952295134  -4.2250799541  -0.8099163671
C  3.0903274909  -2.9441410438  -0.2953813156
C  2.135824836   -1.9545358824  -0.2939423826
C  -0.192558115  -1.1737500521  -0.8399731465
C  -1.442921853  -1.507347197   -1.3373793308
C  -1.7312710598  -2.7980729709  -1.8228572269
C  -0.7645147443  -3.7709110069  -1.8154556363
C  -0.8779540982  3.4228564895   1.178275586
C  -0.3068557856  2.3296763378   0.5254580099
C  1.0154772571   2.3163405775   0.0039840247
C  1.7821061238   3.4550878299   0.1231736968
C  1.215458343    4.5904384949   0.7643482624
C  -0.0662507921  4.5890356829   1.281357086
C  -2.1993862354  3.2322655347   1.6754168876
C  -2.8240440097  2.0122920558   1.5141773391
C  -2.2053124498  0.9137431527   0.8507990582
C  -0.9389164317  1.0770182591   0.331068049
C  0.049436063    0.2010943994  -0.3827079504
C  1.1578982492   0.973506944   -0.5258958191
H  1.3000271002  -5.4737029007  -1.6906810789

```

|                   |               |               |               |
|-------------------|---------------|---------------|---------------|
| H                 | 3.5563373189  | -4.9972732485 | -0.8071715471 |
| H                 | 4.07577961    | -2.74171753   | 0.1090168391  |
| H                 | 2.3734863035  | -0.9808958933 | 0.1147326131  |
| H                 | -2.2088797866 | -0.7440595854 | -1.3925402752 |
| H                 | -2.7199073441 | -3.0102917893 | -2.2140603981 |
| H                 | -0.975710833  | -4.7646402342 | -2.1960344944 |
| H                 | 2.7978764059  | 3.4990052864  | -0.2528431713 |
| H                 | 1.8195464806  | 5.4861982059  | 0.854999457   |
| H                 | -0.453983071  | 5.475758513   | 1.7713498391  |
| H                 | -2.7087286139 | 4.0416518257  | 2.1875271208  |
| H                 | -3.8244639958 | 1.8749278041  | 1.9093827306  |
| H                 | -2.737897684  | -0.0268742365 | 0.7778317419  |
|                   | Core          | RigidRotor    |               |
| SymmetryFactor    | 0.5           |               |               |
| End               |               |               |               |
| Frequencies[1/cm] | 99            |               |               |
| 31.7316           | 49.4290       | 66.2483       |               |
| 138.0046          | 161.8806      | 173.2521      |               |
| 184.5520          | 219.4945      | 235.6287      |               |
| 275.7369          | 307.2856      | 393.1391      |               |
| 417.0060          | 438.2050      | 449.5379      |               |
| 460.1930          | 483.0880      | 516.5071      |               |
| 517.7232          | 534.8959      | 540.8516      |               |
| 558.8324          | 600.1873      | 612.6613      |               |
| 629.4282          | 650.5379      | 654.9675      |               |
| 688.0016          | 690.1003      | 745.5001      |               |
| 748.8926          | 767.8234      | 777.1922      |               |
| 795.0492          | 805.1027      | 814.7514      |               |
| 817.2164          | 830.5157      | 836.6792      |               |
| 882.2554          | 920.2846      | 925.2418      |               |
| 930.9184          | 935.4611      | 969.2119      |               |
| 977.5659          | 985.9808      | 987.7627      |               |
| 993.9605          | 998.7353      | 1035.9238     |               |
| 1047.4599         | 1059.3758     | 1077.1933     |               |
| 1105.2749         | 1143.9525     | 1168.6402     |               |
| 1176.7897         | 1186.4389     | 1197.6183     |               |
| 1206.9548         | 1225.7276     | 1237.9488     |               |
| 1246.5145         | 1251.1115     | 1274.1143     |               |
| 1297.1203         | 1359.1549     | 1374.0799     |               |
| 1386.1984         | 1398.8868     | 1423.6426     |               |
| 1446.2247         | 1451.3189     | 1468.5045     |               |
| 1472.8974         | 1491.4598     | 1513.9921     |               |
| 1541.6924         | 1547.5522     | 1611.1053     |               |
| 1624.4606         | 1632.5483     | 1642.4452     |               |
| 1653.3821         | 1660.7495     | 3157.4570     |               |
| 3161.5664         | 3162.9235     | 3164.1848     |               |

3168.8138                    3176.9933                    3177.5178  
3179.1113                    3182.0634                    3188.6170  
3190.0681                    3191.7599                    3196.5793

ZeroEnergy[kcal/mol]    15.7

ElectronicLevels[1/cm]    1

0    2

End

End

Well            W7   # i7

Species

RRHO

Geometry[angstrom]            35

|   |               |               |               |
|---|---------------|---------------|---------------|
| C | 3.0206219864  | -0.1119912082 | 0.0008346689  |
| C | 4.3085841265  | 0.5103479485  | 0.0004518801  |
| C | 5.4673503688  | -0.3099610389 | -0.0001478937 |
| C | 5.3639925074  | -1.6788900719 | -0.0003521938 |
| C | 4.0909392062  | -2.2920911115 | 0.0000313079  |
| C | 2.9489610514  | -1.5270457211 | 0.000605378   |
| C | 1.8484563393  | 0.7217228665  | 0.0014496334  |
| C | 1.9920857322  | 2.1033058959  | 0.0016519062  |
| C | 3.2652527555  | 2.7018882931  | 0.0012794099  |
| C | 4.3994793798  | 1.9257652607  | 0.0006892245  |
| C | -4.3558185529 | -0.439670975  | 0.0031004635  |
| C | -3.0173464131 | 0.0842782238  | 0.002932485   |
| C | -1.8993928181 | -0.8154522129 | 0.0021887197  |
| C | -2.1381639185 | -2.1830587743 | 0.0016297801  |
| C | -3.4506438222 | -2.6921105355 | 0.00180584    |
| C | -4.5349369644 | -1.8462888988 | 0.0025225375  |
| C | -5.4492105859 | 0.4686663814  | 0.003832778   |
| C | -5.2535433007 | 1.8286167715  | 0.0043799667  |
| C | -3.9351392271 | 2.3655603283  | 0.0042309798  |
| C | -2.9114965461 | 1.4774403887  | 0.0035304677  |
| C | 0.5460791443  | 0.1545192585  | 0.0018259529  |
| C | -0.5771562076 | -0.2997467227 | 0.0020480685  |
| H | 6.4414912376  | 0.1677484166  | -0.0004412932 |
| H | 6.2572478236  | -2.2933079313 | -0.0008055983 |
| H | 4.0170202504  | -3.3737860161 | -0.0001217158 |
| H | 1.9735628921  | -1.9979334656 | 0.0008976582  |
| H | 1.1027891927  | 2.7214841203  | 0.0021136861  |
| H | 3.3432449214  | 3.7830781583  | 0.0014569308  |
| H | 5.3817185832  | 2.3862661575  | 0.0003892828  |
| H | -1.2962479603 | -2.8643342177 | 0.0010451914  |
| H | -3.6003554742 | -3.7657156347 | 0.0013687103  |
| H | -5.5439133075 | -2.2448114868 | 0.0026598636  |
| H | -6.4557946003 | 0.0646515245  | 0.0039549259  |
| H | -6.1019637378 | 2.5045244473  | 0.0049333726  |

```

H   -3.7756190621   3.4381665817   0.0046636249
      Core      RigidRotor
SymmetryFactor  2
      End
Frequencies[1/cm]      99
   8.7262              28.4783              38.7571
  88.9852              92.0995              159.2326
 170.9413              176.5139              209.7582
 231.7899              297.2942              312.9541
 373.5830              393.0787              441.1835
 461.5835              478.3301              478.6445
 484.2257              493.1115              501.7841
 533.0507              552.7103              573.3324
 586.8699              594.0937              611.3175
 634.4992              654.0196              680.0283
 734.2861              746.5449              750.3438
 763.4632              790.0516              797.7234
 805.7023              815.3968              818.7865
 848.0705              880.8097              884.1768
 896.2321              919.2007              924.8919
 966.9394              972.8292              986.4395
 986.8068              998.9686              1006.0310
1039.9596              1045.1873              1073.6857
1088.3464              1110.5837              1164.4961
1168.4275              1179.2270              1184.7178
1192.0571              1204.1274              1230.7032
1238.2763              1240.0708              1280.6737
1334.1925              1341.3724              1356.1784
1358.8128              1391.1092              1402.5784
1428.8494              1454.9322              1465.1617
1470.1596              1493.7238              1508.9227
1543.5731              1582.5397              1611.8681
1622.1835              1625.8853              1652.5847
1660.6859              2289.2682              3159.3298
3159.8429              3163.7105              3163.9641
3170.6640              3170.7308              3180.0661
3180.1994              3182.8304              3183.8319
3194.6651              3195.3638              3195.4530
ZeroEnergy[kcal/mol]   39.1
ElectronicLevels[1/cm] 1
      0      2
      End
      End
Bimolecular   P1      #      P1+H
Fragment      P1
RRHO

```

```

Geometry[angstrom] 34
C      0.000000      1.176058      1.38078
C      0.000000     -1.277307      4.210652
C      0.000000      2.426759      3.445416
C      0.000000      1.277307      4.210652
C      0.000000     -1.176058      1.38078
C      0.000000      0.695870      0.0
C      0.000000      2.397027      2.02356
C      0.000000      0.000000      3.578383
C      0.000000      0.000000      2.183634
C      0.000000     -0.695870      0.0
C      0.000000     -1.176058     -1.38078
C      0.000000      0.000000     -2.183634
C      0.000000     -2.426759      3.445416
C      0.000000     -2.397027      2.02356
C      0.000000     -2.397027     -2.02356
C      0.000000     -2.426759     -3.445416
C      0.000000     -1.277307     -4.210652
C      0.000000      0.000000     -3.578383
C      0.000000      1.176058     -1.38078
C      0.000000      1.277307     -4.210652
C      0.000000      2.397027     -2.02356
C      0.000000      2.426759     -3.445416
H      0.000000     -1.344985      5.293381
H      0.000000      1.344985      5.293381
H      0.000000     -3.391093      3.941387
H      0.000000     -3.331954      1.474123
H      0.000000     -3.331954     -1.474123
H      0.000000     -3.391093     -3.941387
H      0.000000     -1.344985     -5.293381
H      0.000000      1.344985     -5.293381
H      0.000000      3.331954     -1.474123
H      0.000000      3.391093     -3.941387
H      0.000000      3.331954      1.474123
H      0.000000      3.391093      3.941387
Core      RigidRotor
SymmetryFactor 4
End
Frequencies[1/cm] 96
58.52  68.03  126.83  162.58  170.86  194.72  221.46  272.21  273.39
      337.94  354.71  411.11  435.64  458.86  462.68  485.79  506.98  521
      528.11  563.3  585.26  619.92  622.46  642.46  644.92  654.22  692.3
      732.88  744.69  759.78  774.71  782.69  796.05  798.77  812.55
      816.57  826.46  839.98  910.39  919.05  920.95  925.84  939.61
      944.39  972.11  974.54  983.29  984.33  1026.76 1039.13 1061.77
      1062.86 1080.26 1128.47 1162.95 1171.21 1192.72 1204.48 1224.27

```

```

1225.7 1244.76 1250.95 1257.31 1338.12 1360.79 1363.67 1388.74
1409.94 1411.86 1429.94 1448.72 1453.05 1470.29 1483.5 1485.69 1495
1512.34 1515.3 1632.15 1635.03 1644.45 1645.68 1648.5 1659.83
3161.07 3161.42 3161.69 3162.1 3171.84 3172.56 3173.36 3174.09
3184.66 3185.37 3185.46 3186.39
ZeroEnergy[kcal/mol] 0
ElectronicLevels[1/cm] 1
0 1
End
Fragment H
Atom
Mass[amu] 1
ElectronicLevels[1/cm] 1
0 2
End
GroundEnergy[kcal/mol] 14.3
End
Barrier B1 W1 W2 # ts1
RRHO
Geometry[angstrom] 35 #
C 2.258741 -0.129428 0.211456
C 3.512248 0.350380 -0.359126
C 4.622435 -0.534172 -0.561163
C 4.595410 -1.882357 -0.242883
C 3.348864 -2.258452 0.288169
C 2.389982 -1.500075 0.46786
C 1.158982 0.742629 0.416508
C 1.313665 2.063296 0.039166
C 2.512170 2.547973 -0.520934
C 3.590091 1.718169 -0.713369
H 5.526322 -0.113229 -0.990744
H 5.444259 -2.534717 -0.402482
H 0.493501 2.755659 0.16213
H 2.575807 3.593027 -0.802301
H 4.508881 2.101841 -1.143019
C -3.537925 0.036695 -0.418835
C -2.251505 -0.150715 0.112701
C -1.646952 -1.438264 0.306152
C -2.375539 -2.574621 -0.094382
C -3.646875 -2.393731 -0.663544
C -4.230662 -1.14112 -0.829274
C -4.013218 1.371683 -0.451486
C -3.232874 2.394499 0.056082
C -1.943599 2.166678 0.597356
C -1.435584 0.880543 0.598264
C -0.131057 0.246880 1.104455

```

|   |           |           |           |
|---|-----------|-----------|-----------|
| C | -0.415381 | -1.241005 | 0.935508  |
| H | -1.970031 | -3.571917 | 0.029779  |
| H | -4.202419 | -3.270678 | -0.978597 |
| H | -5.222642 | -1.059489 | -1.259832 |
| H | -4.998132 | 1.586301  | -0.852431 |
| H | -3.620274 | 3.407464  | 0.050705  |
| H | -1.399265 | 3.003734  | 1.018031  |
| H | -0.010604 | 0.468207  | 2.176219  |
| H | 0.226095  | -2.019114 | 1.320446  |

Core RigidRotor

SymmetryFactor 0.5

End

Tunneling Eckart

ImaginaryFrequency[1/cm] 40.82

WellDepth[kcal/mol] 54.4

WellDepth[kcal/mol] 4.9

End

Frequencies[1/cm] 98

|       |         |         |         |         |         |         |         |         |      |
|-------|---------|---------|---------|---------|---------|---------|---------|---------|------|
| 38.94 | 85.79   | 120.65  | 164.55  | 173.47  | 177.84  | 216.45  | 246.69  | 250.94  |      |
|       | 316.88  | 405.22  | 413.92  | 423.53  | 447.04  | 458.68  | 466.84  | 481.34  |      |
|       | 508.92  | 516.62  | 528.75  | 538.17  | 553.86  | 578.55  | 604.2   | 606.61  |      |
|       | 622.62  | 659.12  | 679.77  | 695.5   | 718.26  | 745.28  | 749.28  | 766.77  |      |
|       | 781.95  | 791.02  | 810.26  | 829.29  | 834.43  | 855.26  | 866.53  | 874.92  |      |
|       | 913.77  | 923.32  | 948.9   | 956.21  | 972.81  | 981.05  | 983.75  | 993.62  |      |
|       | 1035.14 | 1054.15 | 1070.46 | 1091.78 | 1113.42 | 1128.6  | 1142.42 | 1176.04 |      |
|       | 1177.7  | 1191.74 | 1203.98 | 1211.08 | 1223.44 | 1236.35 | 1240.25 | 1244.28 |      |
|       | 1271.29 | 1304.11 | 1336.28 | 1337.02 | 1368.5  | 1373.29 | 1404.74 | 1423.55 | 1428 |
|       | 1459.19 | 1467.79 | 1473.59 | 1514.87 | 1522.52 | 1576.41 | 1576.93 | 1621.49 |      |
|       | 1633.34 | 1639.58 | 2018.59 | 2970.47 | 3159.62 | 3160.15 | 3160.75 | 3165.84 |      |
|       | 3173.2  | 3176.12 | 3182.55 | 3185.39 | 3186.72 | 3195.16 | 3223.09 | 3225.83 |      |

ZeroEnergy[kcal/mol] 54.4

ElectronicLevels[1/cm] 1

0 2

End

|         |    |    |    |   |     |
|---------|----|----|----|---|-----|
| Barrier | B2 | W2 | W3 | # | ts2 |
|---------|----|----|----|---|-----|

RRHO

Geometry[angstrom] 35 #

|   |           |           |           |
|---|-----------|-----------|-----------|
| C | -2.340307 | -0.099175 | -0.223791 |
| C | -3.687861 | -0.112102 | 0.229538  |
| C | -4.682898 | 0.474762  | -0.609963 |
| C | -4.355807 | 1.046509  | -1.831663 |
| C | -2.990457 | 1.010264  | -2.17466  |
| C | -2.053846 | 0.486106  | -1.472441 |
| C | -1.264466 | -0.648626 | 0.499406  |
| C | -1.522635 | -1.241153 | 1.715805  |
| C | -2.856598 | -1.272733 | 2.198406  |

|   |           |           |           |
|---|-----------|-----------|-----------|
| C | -3.90973  | -0.730178 | 1.489256  |
| C | 3.536565  | 0.714585  | 0.175999  |
| C | 2.331348  | 0.042540  | -0.059104 |
| C | 2.230643  | -1.263178 | -0.624465 |
| C | 3.414595  | -1.913219 | -0.976587 |
| C | 4.642349  | -1.25207  | -0.751739 |
| C | 4.722808  | 0.016763  | -0.194098 |
| C | 3.426612  | 1.999557  | 0.77283   |
| C | 2.180782  | 2.513587  | 1.08557   |
| C | 0.977299  | 1.807357  | 0.823305  |
| C | 1.061479  | 0.559320  | 0.24404   |
| C | 0.048634  | -0.460435 | -0.22583  |
| C | 0.844694  | -1.589154 | -0.668226 |
| H | -5.718676 | 0.472694  | -0.284055 |
| H | -5.119807 | 1.489169  | -2.46019  |
| H | -0.725126 | -1.675582 | 2.307883  |
| H | -3.050416 | -1.740892 | 3.15724   |
| H | -4.915937 | -0.779761 | 1.892219  |
| H | 3.408283  | -2.907053 | -1.409918 |
| H | 5.560590  | -1.761197 | -1.023463 |
| H | 5.692633  | 0.475422  | -0.034031 |
| H | 4.320387  | 2.575945  | 0.986839  |
| H | 2.115614  | 3.494274  | 1.543671  |
| H | 0.022925  | 2.255876  | 1.075194  |
| H | -0.53006  | 0.085046  | -1.26099  |
| H | 0.420373  | -2.519913 | -1.019931 |

Core RigidRotor

SymmetryFactor 0.5

End

Tunneling Eckart

ImaginaryFrequency[1/cm] 1749.68

WellDepth[kcal/mol] 18.2

WellDepth[kcal/mol] 55.9

End

Frequencies[1/cm] 98

|       |         |         |         |         |         |         |         |         |       |  |
|-------|---------|---------|---------|---------|---------|---------|---------|---------|-------|--|
| 37.66 | 50.56   | 61.79   | 165.67  | 167.22  | 183.53  | 204.77  | 222.64  | 232.74  |       |  |
|       | 268.25  | 311.23  | 418.49  | 438.32  | 447.6   | 462.67  | 469.68  | 473.05  |       |  |
|       | 503.95  | 514.45  | 525.65  | 551.16  | 562.55  | 573.1   | 587.22  | 630.55  | 639.1 |  |
|       | 647.63  | 684.98  | 708.31  | 719.76  | 750.19  | 758.25  | 764.69  | 769.81  |       |  |
|       | 783.06  | 812.07  | 818.02  | 832.83  | 837.85  | 843.03  | 898.47  | 905.32  |       |  |
|       | 920.05  | 927.16  | 954     | 977.44  | 980.6   | 980.81  | 986.51  | 1044.93 |       |  |
|       | 1052.63 | 1061.2  | 1070.34 | 1090.13 | 1111.62 | 1134.45 | 1146.82 | 1175.24 |       |  |
|       | 1190.85 | 1200.43 | 1208.68 | 1235.99 | 1243.46 | 1246.42 | 1261.27 | 1286.3  |       |  |
|       | 1314.9  | 1337.44 | 1366.88 | 1382.5  | 1391.02 | 1410.46 | 1427.49 | 1440.49 |       |  |
|       | 1462.53 | 1474.32 | 1483.1  | 1505.02 | 1516.84 | 1555    | 1581.57 | 1599.28 |       |  |

```

1632.27 1643.35 1648.05 1718.34 3155.47 3159.79 3162.18 3162.87
3173.3 3174.75 3176.11 3178.48 3185.38 3186.06 3187.51 3212.4
ZeroEnergy[kcal/mol] 67.7
ElectronicLevels[1/cm] 1
0 2
End
Barrier B3 W3 W4 # ts3
RRHO
Geometry[angstrom] 35 #
C 2.365825 -0.262006 -0.032804
C 3.692473 0.279129 -0.089671
C 4.813725 -0.482144 0.396975
C 4.688264 -1.735288 0.934048
C 3.385019 -2.311123 0.820079
C 2.330605 -1.63187 0.386796
C 1.241945 0.535489 -0.391188
C 1.477744 1.838395 -0.823138
C 2.777777 2.359427 -0.920691
C 3.869763 1.598603 -0.564782
C -3.74794 0.255690 0.285703
C -2.431095 -0.070753 -0.039204
C -2.009947 -1.330091 -0.52616
C -2.966956 -2.305951 -0.71502
C -4.322814 -2.001527 -0.409762
C -4.715982 -0.768972 0.07645
C -3.957923 1.567649 0.797811
C -2.884332 2.421366 0.960377
C -1.551676 2.049425 0.624933
C -1.321852 0.793490 0.102227
C -0.13192 0.013994 -0.335324
C -0.559326 -1.237718 -0.695641
H 5.790434 -0.007574 0.356036
H 5.529823 -2.257195 1.372879
H 2.230566 -2.402399 1.441907
H 0.639864 2.451136 -1.131878
H 2.917323 3.371672 -1.283382
H 4.872173 2.008124 -0.63068
H -2.711203 -3.294249 -1.081967
H -5.071476 -2.771449 -0.560437
H -5.760537 -0.582755 0.302626
H -4.957133 1.893084 1.067365
H -3.055386 3.413591 1.363114
H -0.748085 2.756230 0.796793
H 0.075363 -2.029499 -1.064451
Core RigidRotor
SymmetryFactor 0.5

```

```

End
Tunneling      Eckart
ImaginaryFrequency[1/cm] 1940.52
WellDepth[kcal/mol] 59.2
WellDepth[kcal/mol] 59.9
End
Frequencies[1/cm] 98
33.97 51.1 69.2 138.4 163.21 169.1 174.09 218.65 235.47
275.63 309.29 386 399.41 430.62 441.39 458.94 464.59 471.5
505.97 523.28 536.82 554.87 565.07 589.68 604.33 631.44
635.24 652.93 691.07 695.19 728.73 765.67 768.34 769.55
782.29 789.26 819.78 824.06 832.46 846.51 872.2 898.66
925.27 928.41 935.28 976.3 977.24 982.9 986.1 992.75
1038.66 1040.78 1060.71 1081.64 1096.11 1124.63 1163.54 1173.01
1196.51 1204.1 1216.24 1222.88 1244.21 1254.69 1262.77 1289.08
1312.1 1343.79 1385 1387 1408.55 1425.16 1450.41 1458.51
1481.6 1487.89 1516.15 1519.67 1560.24 1595.23 1623.09 1630.51
1650.35 1657.75 1708.37 2160.33 3146.11 3160.55 3161.66 3162.05
3171.33 3175.01 3178.38 3183.95 3186.59 3186.63 3194.89 3233.27
ZeroEnergy[kcal/mol] 71.0
ElectronicLevels[1/cm] 1
0 2
End
Barrier      B4      W4      W5      #      ts4
RRHO
Geometry[angstrom] 35
C -2.197707 -0.144882 0.064995
C -3.584325 0.107508 -0.149559
C -4.054628 1.429091 0.073082
C -3.189347 2.423468 0.476616
C -1.815584 2.168455 0.68729
C -1.313481 0.893479 0.49732
C -1.691047 -1.425516 -0.193379
C -2.465041 -2.472492 -0.59163
C -3.852466 -2.221894 -0.802308
C -4.394314 -0.974617 -0.588539
H -5.104913 1.650593 -0.086034
H -3.568082 3.426132 0.64178
H -1.167686 2.968541 1.02607
H -2.061235 -3.464318 -0.765263
H -4.486518 -3.034521 -1.142485
H -5.452694 -0.805605 -0.75663
C 3.586967 0.160412 -0.314273
C 2.265109 0.001317 0.108501
C 1.287984 1.030921 0.107675
C 1.660543 2.275205 -0.368749

```

```

C      3.000284      2.469503      -0.797207
C      3.945523      1.460054      -0.774083
C      4.412394      -0.996789      -0.232126
C      3.894248      -2.185569      0.246609
C      2.541759      -2.314352      0.664443
C      1.717206      -1.211508      0.586503
C      0.309843      -0.92734      0.910545
C      0.056939      0.428709      0.617511
H      0.959250      3.099897      -0.422544
H      3.288421      3.450972      -1.157423
H      4.959086      1.657607      -1.106279
H      5.449296      -0.945257      -0.547017
H      4.538083      -3.056359      0.302065
H      2.180864      -3.27292      1.021383
H      -0.259032      -1.513742      1.616954
Core      RigidRotor
SymmetryFactor 0.5
End
      Tunneling      Eckart
ImaginaryFrequency[1/cm]      336.46
WellDepth[kcal/mol]      8.2
WellDepth[kcal/mol]      45.2
End
Frequencies[1/cm]      98
44.46  62.95  101.39  160.88  167.85  175.35  230.55  235.48  282.96  310.1
      399.57  415.89  426.26  460.58  465.68  475.3  507.14  516.44
      529.92  554.61  566.29  571.85  601.37  623.16  635.09  646.2
      679.06  711.11  728.96  747.11  759.14  771.06  777.99  783.91
      802.06  816.6  822.92  838.1  872.83  888.43  910.96  914.6
      918.44  925.56  971.72  976.91  983.38  986.48  997.77  1035.74
      1039.52 1061.1  1071.88 1088.24 1135.11 1162.59 1168.43 1188.01 1198
      1203.36 1209.88 1236.35 1243.37 1249.97 1256.77 1316.94 1347.39
      1360.01 1376.57 1397.68 1405.98 1438.92 1450.76 1451.44 1462.07
      1471.97 1483.26 1511.69 1516.06 1575.03 1620.95 1623.49 1640.4
      1644.66 1654.63 3151.64 3158.47 3161.04 3162.61 3164.03 3171.41
      3172.65 3176.08 3176.72 3184.5  3185.92 3188.54 3212.66
ZeroEnergy[kcal/mol]  19.3
ElectronicLevels[1/cm]      1
0      2
      End
Barrier      B5      W5      P1      #      ts5
RRHO
Geometry[angstrom]      35
C      1.174699      0.053293      1.38532
C      -1.287204      -0.094688      4.200363
C      2.418463      -0.082302      3.44721

```

|   |           |           |           |
|---|-----------|-----------|-----------|
| C | 1.266443  | -0.111489 | 4.208005  |
| C | -1.178943 | 0.056865  | 1.375749  |
| C | 0.699638  | 0.150235  | 0.000000  |
| C | 2.393335  | 0.003653  | 2.0282    |
| C | -0.008257 | -0.061519 | 3.573603  |
| C | -0.003863 | 0.014742  | 2.179755  |
| C | -0.702358 | 0.115351  | 0.000000  |
| C | -1.178943 | 0.056865  | -1.375749 |
| C | -0.003863 | 0.014742  | -2.179755 |
| C | -2.435665 | -0.051903 | 3.433334  |
| C | -2.403012 | 0.023507  | 2.015092  |
| C | -2.403012 | 0.023507  | -2.015092 |
| C | -2.435665 | -0.051903 | -3.433334 |
| C | -1.287204 | -0.094688 | -4.200363 |
| C | -0.008257 | -0.061519 | -3.573603 |
| C | 1.174699  | 0.053293  | -1.38532  |
| C | 1.266443  | -0.111489 | -4.208005 |
| C | 2.393335  | 0.003653  | -2.0282   |
| C | 2.418463  | -0.082302 | -3.44721  |
| H | -1.358108 | -0.156152 | 5.28112   |
| H | 1.330325  | -0.175187 | 5.289053  |
| H | 0.893196  | 2.295542  | 0.000000  |
| H | -3.400775 | -0.07829  | 3.927005  |
| H | -3.336023 | 0.053248  | 1.463489  |
| H | -3.336023 | 0.053248  | -1.463489 |
| H | -3.400775 | -0.07829  | -3.927005 |
| H | -1.358108 | -0.156152 | -5.28112  |
| H | 1.330325  | -0.175187 | -5.289053 |
| H | 3.329171  | 0.033955  | -1.481526 |
| H | 3.380991  | -0.123071 | -3.944897 |
| H | 3.329171  | 0.033955  | 1.481526  |
| H | 3.380991  | -0.123071 | 3.944897  |

Core RigidRotor

SymmetryFactor 1

End

Tunneling Eckart

ImaginaryFrequency[1/cm] 483.3

WellDepth[kcal/mol] 42.8

WellDepth[kcal/mol] 2.5

End

Frequencies[1/cm] 98

|      |        |        |        |        |        |        |        |        |
|------|--------|--------|--------|--------|--------|--------|--------|--------|
| 64.2 | 67.46  | 125.75 | 162.93 | 170.76 | 191.81 | 216.43 | 257.75 | 268.71 |
|      | 274.06 | 306.2  | 337.9  | 361.61 | 415.13 | 435.84 | 460.54 | 464.05 |
|      | 485.83 | 504.75 | 521.08 | 527.89 | 563.09 | 584.35 | 619.12 | 620.87 |
|      | 639.32 | 644.46 | 654.59 | 692.67 | 723.36 | 744.68 | 760.23 | 777.02 |
|      | 781.38 | 786.41 | 799.38 | 812.42 | 816.11 | 829.97 | 841.24 | 909.68 |

918.47 919.06 925.34 940.52 943.95 973.43 975.57 984.08  
 985.07 1027.06 1040.49 1062.72 1063.08 1081.01 1128.25 1163.24  
 1171.56 1192.75 1204.63 1224.14 1225.83 1245.17 1250.97 1253.39  
 1337.31 1345.47 1359.93 1388.7 1409.38 1409.46 1417.13 1446.43  
 1453.49 1465.79 1470.64 1484.5 1492.68 1513.26 1516.33 1631.39  
 1631.7 1641.15 1642.56 1648.33 1658.87 3161.78 3162.05 3162.48  
 3162.8 3173.04 3173.8 3174.52 3175.25 3185.55 3186.21 3186.48  
 3187.31

ZeroEnergy[kcal/mol] 16.8  
 ElectronicLevels[1/cm] 1  
 0 2  
 End

| Barrier            | B6            | W4            | W6           | #             | ts6 |
|--------------------|---------------|---------------|--------------|---------------|-----|
| RRHO               |               |               |              |               |     |
| Geometry[angstrom] |               | 35            | #            |               |     |
| C                  | 0.7847051573  | -2.2807325608 |              | -0.3093406177 |     |
| C                  | 0.6862730475  | -3.6349794426 |              | -0.7519455949 |     |
| C                  | 1.8838825253  | -4.3588916305 |              | -0.992889523  |     |
| C                  | 3.1186764234  | -3.7811717026 |              | -0.8082666708 |     |
| C                  | 3.2237684232  | -2.4368456165 |              | -0.3692368675 |     |
| C                  | 2.0707920001  | -1.7413529612 |              | -0.1377749933 |     |
| C                  | -0.4010965895 | -1.5050922632 |              | -0.0506449821 |     |
| C                  | -1.6283632975 | -2.1147531157 |              | -0.2458952926 |     |
| C                  | -1.7267291917 | -3.453538915  |              | -0.6839171957 |     |
| C                  | -0.6027017268 | -4.2021237276 |              | -0.932918803  |     |
| C                  | -0.9809142482 | 3.2935342619  |              | 1.5362806318  |     |
| C                  | -0.4504583898 | 2.0687427222  |              | 1.1269093695  |     |
| C                  | 0.9418528841  | 1.8019026231  |              | 1.0274692636  |     |
| C                  | 1.8294266375  | 2.8057007545  |              | 1.3518427116  |     |
| C                  | 1.3146835084  | 4.0625973805  |              | 1.7714295607  |     |
| C                  | -0.0404194881 | 4.3126714653  |              | 1.8652571878  |     |
| C                  | -2.4007982936 | 3.3811098632  |              | 1.5779620461  |     |
| C                  | -3.1635597563 | 2.2875524614  |              | 1.2241625054  |     |
| C                  | -2.5885660159 | 1.0526517709  |              | 0.8112814968  |     |
| C                  | -1.2146567814 | 0.9305019678  |              | 0.7575968952  |     |
| C                  | -0.2204796632 | -0.1260841497 |              | 0.4003008898  |     |
| C                  | 1.0206291598  | 0.4238183059  |              | 0.5709685137  |     |
| H                  | 1.8097489515  | -5.3878033113 |              | -1.3291390934 |     |
| H                  | 4.0210925575  | -4.3522762599 |              | -0.9980587894 |     |
| H                  | 4.1992451422  | -1.9854761541 |              | -0.2251252217 |     |
| H                  | -2.5412610987 | -1.5657740354 |              | -0.0631673097 |     |
| H                  | -2.7096791537 | -3.8894250164 |              | -0.8233202922 |     |
| H                  | -0.6856442663 | -5.2301517298 |              | -1.2692391836 |     |
| H                  | 2.9018981638  | 2.656471269   | 1.2937275693 |               |     |
| H                  | 2.0157505846  | 4.8497365591  | 2.0257779792 |               |     |

|                          |               |               |              |
|--------------------------|---------------|---------------|--------------|
| H                        | -0.3917487338 | 5.2862844173  | 2.189997336  |
| H                        | -2.8797421392 | 4.304102655   | 1.8871711446 |
| H                        | -4.2447612462 | 2.3627009879  | 1.2592940006 |
| H                        | -3.2564586757 | 0.2417555151  | 0.5508018049 |
| H                        | 1.9550215897  | -0.4921623879 | 0.2686295241 |
|                          | Core          | RigidRotor    |              |
| SymmetryFactor           | 1             |               |              |
|                          | End           |               |              |
|                          | Tunneling     | Eckart        |              |
| ImaginaryFrequency[1/cm] |               |               | 1643.4590    |
| WellDepth[kcal/mol]      |               | 13.3          |              |
| WellDepth[kcal/mol]      |               | 8.7           |              |
|                          | End           |               |              |
| Frequencies[1/cm]        | 98            |               |              |
| 33.5701                  | 56.1414       |               |              |
| 126.3923                 | 143.4692      | 156.0089      |              |
| 171.0668                 | 213.9672      | 236.8827      |              |
| 243.6020                 | 289.8518      | 297.6172      |              |
| 399.3287                 | 423.0343      | 455.8833      |              |
| 456.6240                 | 461.2426      | 470.0646      |              |
| 514.2527                 | 523.9110      | 537.5632      |              |
| 562.8564                 | 566.3144      | 602.6219      |              |
| 622.8504                 | 636.1367      | 637.4497      |              |
| 653.5998                 | 694.1796      | 702.4795      |              |
| 747.1855                 | 749.2640      | 768.5140      |              |
| 771.4751                 | 783.2569      | 802.3337      |              |
| 814.8253                 | 815.5876      | 834.4071      |              |
| 869.6320                 | 884.7928      | 903.0485      |              |
| 916.3481                 | 921.5954      | 923.5672      |              |
| 971.6840                 | 975.0748      | 983.6243      |              |
| 985.3660                 | 1003.2209     | 1006.2362     |              |
| 1039.7883                | 1053.7655     | 1064.5812     |              |
| 1083.6640                | 1100.7463     | 1160.3098     |              |
| 1167.3041                | 1184.7175     | 1200.6906     |              |
| 1207.8662                | 1216.8740     | 1238.4415     |              |
| 1244.2767                | 1254.7959     | 1263.9597     |              |
| 1310.1973                | 1352.9952     | 1375.8493     |              |
| 1378.2890                | 1399.4309     | 1403.8065     |              |
| 1444.2837                | 1449.1679     | 1453.8208     |              |
| 1471.2053                | 1479.2377     | 1500.9410     |              |
| 1514.5993                | 1519.0154     | 1590.5581     |              |
| 1624.8215                | 1627.4298     | 1630.5499     |              |
| 1642.0885                | 1655.3031     | 1668.5165     |              |
| 3157.5171                | 3162.0513     | 3162.3131     |              |
| 3162.8564                | 3168.8741     | 3174.4213     |              |
| 3178.2756                | 3180.2589     | 3181.9027     |              |

```

3186.0886          3194.4833          3220.6036
ZeroEnergy[kcal/mol]  24.4
ElectronicLevels[1/cm]  1
0      2
  End
  Barrier      B7      W6      W7      #      ts7
  RRHO
Geometry[angstrom]      35      #
C  0.4453019587 -2.4051883501 -2.438972702
C  0.0242437831 -3.7239504533 -2.8034695411
C  0.6971503262 -4.3949126872 -3.858028866
C  1.7362343207 -3.7971643462 -4.5268696321
C  2.1483187486 -2.4945468842 -4.1691731556
C  1.518852218 -1.8163190372 -3.1522428369
C  -0.2418135909 -1.7351389751 -1.3636386572
C  -1.28931124 -2.3772214471 -0.7188570874
C  -1.6934994328 -3.6724154951 -1.0910201727
C  -1.0523012609 -4.3335174542 -2.1099426828
C  0.1546580916 -0.4232226569 -0.9528487414
C  0.9456560219 0.5310807217 -0.7523835256
H  0.3725291425 -5.3948059442 -4.1264860238
H  2.2415249495 -4.3209202116 -5.3304446338
H  2.966960883 -2.0255827174 -4.7033817853
H  1.8386129716 -0.8177798273 -2.8833319693
H  -1.7919079771 -1.8669179098 0.092907926
H  -2.5134238828 -4.1450527932 -0.562520997
H  -1.3600686903 -5.3329462166 -2.3984092272
C  -1.1494684194 3.2708183011 0.5271451903
C  -0.6423643646 2.0439253773 0.0324483613
C  0.7433905566 1.8649416333 -0.2635081753
C  1.6186627246 2.9088581831 -0.0593296973
C  1.1218644175 4.138769047 0.4409158155
C  -0.2136348282 4.3237229544 0.7271789569
C  -2.547659124 3.3458182904 0.7732270498
C  -3.3647448812 2.2639031855 0.5285422228
C  -2.8466859167 1.0324247526 0.0252859504
C  -1.5049303961 0.9683675418 -0.1937785795
H  2.673877841 2.7970097408 -0.2772110042
H  1.8175995582 4.9550589088 0.5992386128
H  -0.5617119616 5.278682709 1.1067118202
H  -2.9706415496 4.2693290497 1.1539833943
H  -4.4304965212 2.3406518031 0.7173333878
H  -3.516203476 0.2019252069 -0.1695839947
  Core      RigidRotor
SymmetryFactor 0.5
  End

```

| Tunneling                | Eckart    |           |
|--------------------------|-----------|-----------|
| ImaginaryFrequency[1/cm] |           | 401.3343  |
| WellDepth[kcal/mol]      | 37.4      |           |
| WellDepth[kcal/mol]      | 14.0      |           |
| End                      |           |           |
| Frequencies[1/cm]        | 98        |           |
| 17.7953                  | 43.3457   |           |
| 54.4185                  | 117.9750  | 163.4918  |
| 165.4421                 | 175.6762  | 196.3896  |
| 228.1236                 | 277.5567  | 300.5602  |
| 385.4610                 | 410.6787  | 431.1354  |
| 454.1229                 | 466.0866  | 478.0993  |
| 500.0272                 | 502.8386  | 505.8946  |
| 534.2144                 | 545.2254  | 580.9751  |
| 584.4129                 | 591.8494  | 601.4257  |
| 633.3467                 | 650.6032  | 679.4575  |
| 734.5557                 | 748.2382  | 756.2870  |
| 769.8891                 | 789.3377  | 801.9103  |
| 805.0276                 | 817.0028  | 818.7011  |
| 864.4040                 | 882.6355  | 886.1804  |
| 893.8200                 | 917.4774  | 930.9143  |
| 971.1969                 | 972.4378  | 985.7269  |
| 988.4417                 | 1001.2893 | 1009.8284 |
| 1030.0972                | 1046.4730 | 1061.8220 |
| 1078.8458                | 1107.9584 | 1164.0445 |
| 1168.9914                | 1181.4204 | 1186.6101 |
| 1198.0531                | 1205.2740 | 1227.7192 |
| 1238.2474                | 1242.2359 | 1276.2980 |
| 1302.1298                | 1350.4984 | 1355.4473 |
| 1387.4974                | 1391.6175 | 1414.9456 |
| 1425.1632                | 1449.8530 | 1459.1807 |
| 1466.8844                | 1490.5078 | 1510.5383 |
| 1543.6829                | 1585.6855 | 1609.7500 |
| 1626.2875                | 1632.5821 | 1651.7136 |
| 1660.0021                | 1949.2553 | 3156.8031 |
| 3159.8074                | 3162.4511 | 3164.2072 |
| 3170.2133                | 3170.9565 | 3178.6809 |
| 3180.4209                | 3181.1394 | 3185.4943 |
| 3193.6358                | 3198.6869 | 3199.9465 |
| ZeroEnergy[kcal/mol]     | 53.1      |           |
| ElectronicLevels[1/cm]   | 1         |           |
| 0                        | 2         |           |
| End                      |           |           |
| End                      |           |           |